Separation and Purification Technology 377 (2025) 134463

Contents lists available at ScienceDirect

Separation and Purification Technology

journal homepage: www.elsevier.com/locate/seppur

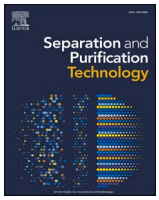

Rapid multi-criteria screening of energy-integrated distillation processes for nonideal mixtures

Momme Adami [a], Dennis Espert [a], Mirko Skiborowski [a,b,*]

[a] Hamburg University of Technology, Institute of Process Systems Engineering, Am Schwarzenberg-Campus 4, 21073 Hamburg, Germany
[b] United Nations University Hub on Engineering to Face Climate Change at the Hamburg University of Technology, United Nations University Institute for Water, Environment and Health (UNU-INWEH), Hamburg, Germany

ARTICLE INFO

Editor: Cintia Marangoni

Keywords:
Distillation
Shortcut screening
Thermal coupling
Heat integration
Vapor recompression
Dividing Wall Column
Process intensification

ABSTRACT

Several thousand distillation columns are industrially employed for various separations, accounting for a substantial share of the industrial energy demand. In order to reduce their energy requirements various means for energy integration, such as direct heat integration, multi-effect distillation, thermal coupling, or vapor recompression can be applied. Considering these options and combinations of these, several hundred possible process configurations can be designed even for separations into three product streams, while the choice for a best option depends strongly on the specific separation task and system properties. In order to enable a reliable case-specific evaluation, which avoids simplified heuristics or simplified thermodynamics, this article presents a computationally efficient, algorithmic framework for a multi-criteria evaluation of more than 750 energy-integrated distillation sequences for multicomponent separations in three product streams. The framework employs thermodynamically sound pinch-based shortcut models that do not rely on constant relative volatility and constant molar overflow assumptions, making it applicable to nonideal and azeotropic mixtures. Based on the minimum energy duties and the respective flowsheet information, classical estimation methods for equipment sizes, operating costs, and capital investment, are employed. Several case studies demonstrate the framework's applicability to azeotropic systems, its computational efficiency benefits that enable performing sensitivity analyses for varied process, thermodynamic, and economic scenarios.

1. Introduction

To effectively mitigate climate change, reducing the energy consumption and greenhouse gas emissions of the chemical industry is imperative, as it ranks among the largest sources of global industrial emissions [1]. A significant portion of these emissions originates from energy-intensive thermal separations, particularly distillation processes, which are prevalent due to their ability to produce high-purity products at large scales [2]. With over 40,000 distillation columns in operation, accounting for more than 90 % of all fluid separations [3,4], distillation substantially contributes to global industrial energy demand. While technologies such as membranes offer potential solutions for certain applications, distillation is not inherently energy-inefficient [5] and theoretical studies have shown that other technologies do not easily outperform it under ideal conditions [6]. Nonetheless, numerous energy integration techniques have been developed to enhance the energy efficiency of distillation processes [7], especially the separation of multicomponent mixtures that typically require a sequence of distillation columns. The most prominent options are direct heat integration (HI), multi-effect distillation, thermal coupling and heat-pump assisted distillation, most prominently in vapor recompression designs [8].

Direct HI can be accomplished between the reboiler and condenser of different columns in case there is a sufficient driving force, i.e. a positive temperature difference between the top vapor stream of the column that provides heat and the bottoms stream of the column that is supposed to take up heat. In column sequences for three product separations, HI may be achieved by adjusting the pressure in at least one column such that the top temperature of the heat-supplying column is higher than the bottom temperature of the heat-receiving column[9]. Typically, the heat demand of the column with the smaller duty can be fully integrated, while a reduced amount of external utility remains necessary for the other column. In case both columns have similar duties, HI can reduce

* Corresponding author at: Hamburg University of Technology, Institute of Process Systems Engineering, Am Schwarzenberg-Campus 4, 21073 Hamburg, Germany.
E-mail address: mirko.skiborowski@tuhh.de (M. Skiborowski).

https://doi.org/10.1016/j.seppur.2025.134463
Received 28 May 2025; Received in revised form 14 July 2025; Accepted 21 July 2025
Available online 23 July 2025

the net energy demand by up to 50 %.

Multi-effect distillation extends the concept of direct HI by e.g. dividing the feed stream among multiple columns conducting the same separation at different pressures [8]. If a binary separation is performed by two (three) such integrated columns, this is also referred to as dual (triple) effect distillation. A variant of multi-effect distillation involves gradually increasing the purity of one of the products over multiple columns to obtain a cascade of product temperatures, thereby lowering the required pressure modifications for HI [10]. The net energy demand of multi-effect sequences is approximately that of the conventional separation divided by the number of utilized effects, offering substantial energy-saving potential at the cost of increased investment for a larger number of columns. While a dual effect distillation can potentially reduce the net energy demand by 50 %, the added effect of additional columns decreases with gradually. Multi-effect distillation processes with up to four effects have been proposed for methanol distillation [11] and in seawater distillation, which employs single stage distillation/evaporation, even multi-effect distillation plants with up to 16 effects have been established [12].

Another classical means for reducing the exergy losses in distillation columns are thermal couplings of distillation columns, for which heat exchangers and liquid streams between adjacent distillation columns are replaced by bidirectional liquid and vapor transfer, effectively combining energy and mass integration [13,14]. A notable example of this process intensification is the equipment-integrated dividing wall column (DWC), which consolidates multiple separations within a single column shell. More than 300 industrial-scale implementations of DWC have been reportedly demonstrated significant benefits [15], enabling 25–40 % lower energy requirements due to reduced exergy losses and a smaller process footprint, as well as up to 30 % lower investment costs resulting from a decreased number of equipment [16,17]. Nonetheless, despite these advantages, it is important to recognize that DWC and other thermally coupled sequences have limitations, such as the constraint of operating at a single pressure and the challenge of managing a larger temperature span across the column as energy is supplied or removed at more extreme temperature levels [18]. Thermal coupling without vapor transfer, also termed liquid-only transfer configurations retain the heat exchanger for an extended column section [19] and preserve the energy-saving benefits of thermally coupled connections while hydrodynamically decoupling the columns [20]. This can provide additional operational flexibility and allow for further HI [18,21].

Due to its potential for electrification heat-pump assisted distillation is currently receiving increased attention. Mechanical vapor recompression (VRC) is a popular heat-pump concept in which the top vapor stream of a column is compressed to provide its heat of condensation at an increased temperature. In that sense the overhead vapor as the working fluid in an open Clausius-Rankine cycle [22]. Other approaches include closed-cycle heat pumps with freely selectable working fluids [23,24]. The use of electric compressors offers the unique opportunity to transform a thermally driven process into an electrically driven one while significantly improving energy efficiency [5]. Although heat pumps can yield some of the highest energy savings, on the necessity for expensive compressors represents an economic burden that limits their attractiveness for short-term investments. The efficiency of heat pumps is typically measured by the coefficient of performance, which depends strongly on the temperature lift. A lower temperature lift results in a higher coefficient of performance, making heat pumps especially efficient for separating close-boiling mixtures. However, they can still achieve significant energy savings for larger temperature lifts [24] and can be effectively applied across multiple columns [25]. Yet, similar to multi-effect distillation, VRC can also be applied for an individual distillation column. Despite these advancements, heat pump applications remain subject to several practical limitations. The compressor discharge temperature and pressure ratio are limited by mechanical constraints, the coefficient of performance must be sufficiently high to be economically viable and, if process medium servers as working fluid, it must be suitable for compression. In particular, if the process medium is prone to polymerization, thermal degradation, or fouling, this restricts the use of open compression cycles.

Although all of the above-mentioned energy integration concepts can reduce the net energy requirements and costs compared to conventional distillation processes, it is not trivial to decide which of them is the best choice for a specific separation problem. Unfortunately, few design methodologies evaluate competing integration methods simultaneously, which restricts the ability to identify the most attractive alternatives. Additionally, the combination of multiple energy-integration concepts, such as thermal coupling and VRC [26], is rarely explored beyond individual solutions, yet it can significantly increase saving potential but also the number of possible flowsheets. Moreover, the actual savings and best flowsheet options depend heavily on the specific separation task, necessitating case-specific evaluations that cannot be adequately addressed with heuristics. Therefore, a simultaneous comparison of a broad range of energy integration concepts is crucial to accurately assess their savings potential and identify the flowsheets of highest interest for a specific separation task. Cui *et al.* [27] highlighted this need by applying shortcut calculations to quickly choose between heat–pump–assisted and multi–effect distillation for five binary systems, yet their study was restricted to those two options.

So far, a few approaches have been developed to address the challenge of evaluating and selecting between the multitude of energy integration concepts and possible flowsheets, varying in scope, methodology, and the extent to which they consider different integration techniques. For instance, Kiss *et al.* [28] presented a selection scheme for heat pump-assisted distillation concepts based on an extensive literature review, providing heuristic guidelines for choosing appropriate heat pump configurations under different process conditions. Unlike the knowledge-based approach of Kiss *et al.* [28], Gooty *et al.* [5] present a detailed analysis of the efficiency of binary distillation with various intensification methods, specifically analyzing the thermodynamic efficiency under consideration of ideal mixtures with constant relative volatilities.

Especially Agrawal and co-workers have contributed heavily to the understanding of energy-efficient distillation processes, also presenting elaborate process synthesis methods that effectively generate all possible simple sequences and thermally coupled configurations for the separation of zeotropic mixtures [29]. In more recent work, the methods were also extended and demonstrated for multicomponent separations that do not mandate the separation of each individual component [30,31]. Agrawal [32] synthesized all basic configurations of conventional columns and feasible thermally coupled schemes, including non-sharp separations. Similarity, Jiang *et al.* [33] extended the matrix-method by Shah and Agrawal [34] for synthesizing conventional and thermally coupled column configurations with non-sharp separations, providing a systematic way to explore configuration options. By further integrating performance models, based on the well-known Underwood equations, Nallasivam *et al.* [35] pursued a full-enumeration combined with a global minimization of the vapor duty of each configuration resulting from the basic and thermally coupled distillation configurations. The optimization framework was later extended for the minimization of exergy losses [36], as well as an estimate of the total annualized cost (TAC) [37], estimating the minimum number of theoretical stages by

$$N_{min} = \frac{ln\left(\frac{x_{L,D}}{x_{H,D}}\frac{x_{H,B}}{x_{L,B}}\right)}{ln(\alpha_{LH})}, \tag{1}$$

applying the well-known Fenske equation [38]. The estimation builds on the compositions of the liquid phase x of the distillate D and bottoms product B of light (L) and heavy (H) key components, considering a constant relative volatility α_{LH} between them. The improved reformulations of the Underwood equations and the developed optimization

framework enables a rigorous evaluation of complex thermally coupled configurations even for multicomponent mixtures with five or more products [39], but the assumption of constant relative volatilities does limit the applicability to real mixtures with non-ideal thermodynamics.

Complementary strategies by other research groups combine shortcut evaluations and metaheuristic optimization to explore various integration concepts. A shortcut-based comparison for multi-effect distillation and VRC for binary separation problems is e.g. presented by Cui *et al.* [27], concluding that multi-effect distillation shows beneficial performance for mixtures with high relative volatilities, whereas heat pumps are better suited for mixtures with low relative volatilities. Wei-zhong and Xi-Gang [40] employed simulated annealing to optimize heat-integrated distillation sequences, but their study did not consider any other type of energy integration. Zhang *et al.* [41] also employed simulated annealing to optimized thermally coupled sequences with simultaneous consideration of direct HI. Li *et al.* [42] proposed a superstructure-based framework that accounts for simple and thermally coupled column configurations, considering all heat–integration possibilities via a mixed–integer linear–programming (MILP) transportation model: At each step of an outer simulated annealing search, the flowsheet is fixed, its reboiler and condenser duties form a source–sink matrix, and a transshipment–style MILP chooses the hot–cold matches that satisfy temperature and capacity constraints The resulting hierarchy is however computationally intensive, taking about 19 h for a single separation task.

Importantly, all previously discussed methods fundamentally build on the Underwood equations or improved formulation, which nevertheless all assume constant molar overflow and constant relative volatilities to estimate the minimum energy demand (MED) of a given separation [43–45]. While this shortcut approach enables computationally efficient solutions as well as global optimization for advanced model formulations [35,36], the constant molar overflow and constant relative volatilities assumptions may result in significant inaccuracies for non-ideal systems. Cui *et al.* [27] have validated their results for ideal systems with rigorous studies similarly to Ramapriya *et al.* [46], who have shown that shortcut-based optimization results obtained within less than a minute for 18 simple and thermally coupled configurations agree well with rigorous studies performed with Aspen Plus in months of manual efforts. However, the respective evaluations were performed for fairly ideal systems. Mathew *et al.* [47] recently showed how the assumption of constant molar overflow can effectively be relaxed, yet the constant relative volatilities assumption remains essential to the Underwood-based methods, maintaining a limiting factor.

To overcome these limitations, rigorous simulation-based approaches have been applied to evaluate and optimize distillation configurations, including various energy integration concepts. Tang and Ward [48] conducted simulations using Aspen Plus's RadFrac model for the direct and indirect sequences, side rectifier, side stripper and the respective liquid-only transfer and directly heat-integrated variants as well as DWC and optimized TAC using simulated annealing. Gan *et al.* [25] extended this work focusing solely on VRC variants and evaluated a total of 29 process configurations, while Mekidiche *et al.* [49] recently performed a simulation/optimization-based evaluation of 77 process configurations, including heat-pump-assisted distillation and combinations with thermal coupling and direct HI based on rigorous column models in Aspen Hysys. Based on an initial simulation-based assessment of all variants, the most promising are further optimized by means of a particle swarm optimization approach for minimum TAC while accounting for pressure drops. Despite obtaining efficient process designs and accommodating non-ideal thermodynamics, such rigorous simulations are time-consuming due to being computationally intensive, demanding computational times of several hours or even days [50]. This limits their practicality for screening a large number of configurations as well as different scenarios, considering e.g. different feed conditions, thermodynamic properties or cost parameters. While metaheuristics do enable a global search and can overcome local optima, it is also important to acknowledge that they do not provide any proof of optimality, not even local optimality. Therefore, such stochastic optimizations should always be repeated to check for reliability. Consequently, despite the necessary simplifications, shortcut models provide essential benefits for the fast identification of suitable process variants during conceptual design, whereas more rigorous models can be applied for the most promising options in detailed design stages [51,52]. For theses designs, rigorous superstructure optimization models have been presented that guarantee at least locally optimal equipment design and operational parameters [17,53,54].

While a number of thermodynamically sound shortcut methods are available that effectively avoid constant molar overflow and constant relative volatilities assumptions [55], only few have been applied for energy-integrated distillation processes. Brüggemann and Marquardt [56] first applied the Rectification Body Method for the screening of several simple and thermodynamically-coupled process configurations. The framework was later expanded by Skiborowski [57] to cover HI, as well as several options for multi-effect distillation and VRC, covering about 20 different process configurations. In more recent work also some liquid-only transfer configurations with HI were evaluated to analyze the potential of a combined thermal coupling and HI for side rectifier and side-stripper configurations [58,59]. All these evaluate the process configurations solely on the basis of the minimum energy demand and respective operating costs, which directly scale with energy consumption and depend mainly on the price of the utilized utilities, especially steam and electricity. Although energy demand can provide a rough estimation of capital costs, since higher energy requirements often indicate more challenging separations that necessitate additional stages, larger vapor flows, increased column diameters, and larger heat exchanger areas [60] it does not provide a full coverage of the total annualized costs. In particular, it does not account for the number and size of columns and heat exchangers, the significant investment in compressors, or variations in temperature differences and other operating conditions. To enable a more accurate economic evaluation, it is imperative to consider the trade-off between operating and capital costs during conceptual design.

To address these challenges in a computationally efficient manner, the previously proposed shortcut screening approach for energy-integrated distillation processes [57] has been extended to cover all simple sequences, direct HI options, multi-effect distillation with two and three effects, thermal coupling, as well as all combinations with VRC, for the separation of a given mixture into three product streams. Thus, in total up to 750 process configurations with individual and hybrid energy integration schemes are evaluated. The multi-criteria evaluation builds on the computed minimum energy demand and operating cost calculations, but extends to the capital costs determined by a modified version of the Fenske equation that does not require limiting constant relative volatilities assumptions [61] in combination with Guthrie's method for capital cost estimation [62,63]. This also allows for the combined evaluation of the TAC estimates.

The computational framework is described in detail in Section 2, while the framework's capabilities are demonstrated for two case studies in Section 3. The well-known separation of benzene, toluene, and p–xylene is presented in Section 3.1 and illustrates the framework's computational efficiency, enabling effective sensitivity analyses with respect to uncertain operating conditions, thermodynamic models and feed specifications. The second study in Section 3.2 addresses the separation of a the quaternary azeotropic mixture of acetone, chloroform, benzene, and toluene into three product fractions, demonstrating the applicability of the framework to highly nonideal systems. The influence of utility prices and the capital charge factor on the economic performance of different energy integration concepts are analyzed in order to identify the most promising process alternatives under varying market conditions. Section 4 finally provides a conclusion and an outlook on further work to expand the application range of the framework.

2. Shortcut screening framework

The algorithmic framework for the automatic evaluation of energy-integrated distillation processes is illustrated in Fig. 1. The MATLAB-based screening tool automatically evaluates various distillation-based separation processes for the separation of a homogeneous multicomponent mixture, requiring three individual inputs:

1. The separation problem specification needs to define the feed composition and flow rate as well as product composition and base operating pressure. For the current implementation of the screening all feed and product streams are assumed to be saturated liquids at the respective pressure levels.
2. Thermodynamic property data for the given chemical system is supplied as a text file in a consistent format, which can e.g. be extracted from Aspen Plus using a dedicated report file parser.
3. Utility and cost data, required to estimate the operating and investment costs on the basis of the performance evaluation.

While the main body of the screening tool that is the topic of the current publication is implemented in MATLAB, all thermodynamic property computations, as well as minimum energy demand computations for individual splits with the Rectification Body Method [64] are performed via MEX-functions implemented in C-Code. The MEX-functions are supplied as part of the process synthesis software collection of AVT.SVT at RWTH Aachen University [65]. This includes common thermodynamic models, such as DIPPR correlations for specific heat capacities and heat of vaporization, the Antoine equation for vapor pressure computations and NRTL, Wilson, UNIQUAC G^E-models, or the Redlich-Kwong equation of state.

Based on this backbone, the individual process configurations are defined in the screening tool as subsequently described in Section 2.1. For each process configuration, all relevant mass and energy streams, temperatures and pressures are determined, as well as the minimum net energy demand (cf. Section 2.2), defined as the sum of all externally supplied heat and electricity. In multicomponent mixtures, phase transitions occur over a range of temperatures due to the differing boiling points of the individual components – a phenomenon known as temperature glide. To accurately represent this behavior, bubble and dew points of affected process streams are determined via flash calculations at saturated liquid or saturated vapor conditions, rather than assuming constant temperatures during phase change as in some previous approaches [56,57]. If the operating parameters have degrees of freedom, as e.g. the split in the prefractionator, these are optimized to minimize the net energy demand of the configuration (cf. Section 2.3).

In addition to mass and energy evaluations, the framework performs a comprehensive cost calculation, which is described in Section 2.4. Operating and capital costs are calculated separately and then combined to yield the total annual cost, based on a specified utility network and predefined cost parameters. The dimensions of each piece of equipment are estimated to calculate the capital costs. Finally, the results can be examined graphically to evaluate the performance of different process alternatives.

2.1. Individual process configurations

The individual process configurations all perform a separation of the given feed stream into the three distinct products streams. For such a separation, a sequence of at least two columns is typically required, unless a simple side stream column would be sufficient. As these are usually restrained in terms of product purity [66], they are not considered in the current screening, which focusses on the separation of three product streams in respect to sharp splits.

The following subsections provide an overview of the individual process configurations which are not restricted in terms of the number of components, but require the specification of a light boiling fraction A, medium boiling fraction B and heavy boiling fraction C as the three distinct product streams. It is important to note that these product streams have to represent sharp splits or highest-purity splits [55], to derive accurate estimates by means of the pinch-based shortcut methods. The framework covers simple and thermally coupled configurations, as well as direct HI and multi-effect configurations. For each of

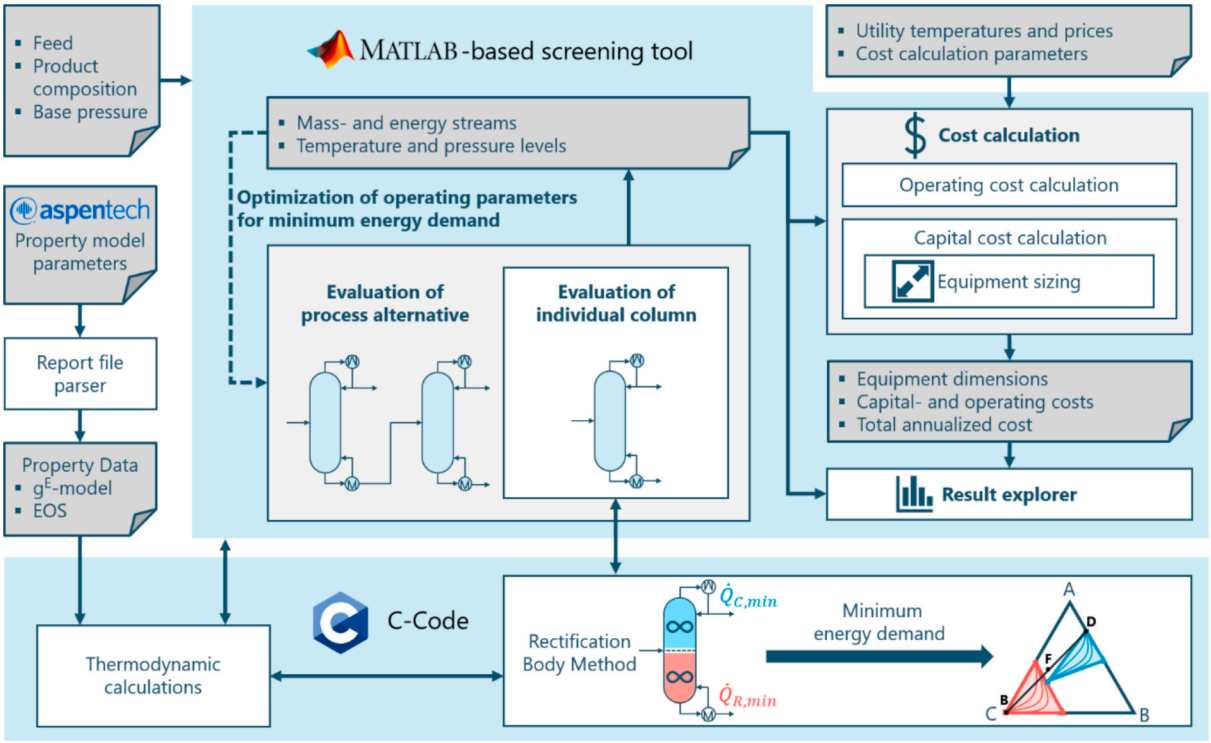

Fig. 1. Schematic of algorithmic framework for fast automatic evaluation of energy-integrated distillation processes.

the resulting 78 process configurations additional vapor recompression options are considered for integration of the condenser and reboiler of an individual column as well as those of other columns, resulting in over 750 different process configurations.

2.1.1. Simple column configurations

The three simple sequences of conventional columns for the ternary separation of a homogeneous feed stream into three product fractions include the direct and indirect sequence, which both utilize two columns, and the sloppy split (also called intermediate split) which eliminates one of the fractions from each of the first column's product streams and requires three columns in total.

2.1.2. Thermally coupled configurations

Thermal coupling of distillation columns is achieved by exchanging an interconnecting stream and the respective reboiler or condenser by a bidirectional liquid and vapor transfer. Six thermally coupled configurations can be derived from the simple sequences described in Section 2.1.1. The thermally coupled direct and indirect sequence result in the well-known side rectifier and side stripper configuration. Four prefractionator configurations are further derived by partial to full thermal coupling of the sloppy split sequence, as illustrated in Fig. 2. The basic prefractionator configuration results from the partial thermal coupling of the second and third column in the sloppy split sequence, which is illustrated as prefractionator with individual reboiler and condenser connected to a main column with a side stream. The other three prefractionator configurations result from further thermal coupling for the two interconnecting streams between the prefractionator and the main column. If both interconnecting streams are replaced by thermal couplings, the resulting fully thermally coupled prefractionator is also termed Petlyuk-configuration. The side rectifier and side stripper, as well as the Petlyuk configuration may all be implemented as dividing wall columns to spare some additional investment cost. For that only the cost of the main column is considered while the prefractionator is assumed to be integrated into the main column's shell. No additional cost factors are included for the section with the dividing wall.

The computation of the minimum energy duty for each of the thermally coupled configurations is based on the decomposition approach proposed by Carlberg and Westerberg [67] and follows the same implementation for the Rectification Body Method, as described by Brüggemann and Marquardt [56].

The bidirectional transfer of liquid and vapor between the coupled columns is approximated by means of subcooled or superheated net streams, which serves as a proper estimate with negligible errors as shown by Navarro *et al.* [68]. The transition from a direct and indirect sequence to a side stripper and side rectifier with their respective models via thermal coupling and equivalent arrangement of the column sections is shown in Fig. 3. The side rectifier is modeled as a direct sequence of which the feed stage of the second column is heat integrated with the reboiler of the first column. Thus, the heat demand of the first column is fulfilled by the second column. Similarly, the side stripper is modeled as an indirect sequence of which the feed stage of the second column is heat integrated with the condenser of the first column, so that the cooling demand of the first column is fulfilled by the second column. Thermally coupled connections between the prefractionator and the main column of the prefractionator configuration are modeled similar as for the side rectifier and side stripper. No additional heat exchanger costs are considered for thermally coupled streams.

The minimum energy demand of the main column in the prefractionator configuration is determined by considering it as two subcolumns which are fully heat-integrated at the opposing ends as depicted in Fig. 4. Each of the sub-columns performs a binary separation with identical product composition at the interconnection, which is the bottom of the top sub-column and the distillate from the bottom subcolumn. The sum of the respective products represents the side stream of the main column. The combination of both columns is operated at the lowest reboiler duty that fulfills the vapor demands of both sub-columns, which is determined from a univariate optimization (cf. Section 2.3). The applicability of this model requires that the upper feed contains only light and middle boiling fraction and the lower feed contains only middle and heavy boiling fractions, which has to be assured by a proper split performed in the prefractionator.

2.1.3. Directly heat integrated configurations

The previously shown sequences with two or more hydrodynamically decoupled columns can benefit from direct heat integration, which utilizes the condenser duty of one column to provide this heat for the evaporation in the reboiler of an adjacent column. For this, the pressure in at least one of the columns needs to be adjusted, such that the top temperature of the heat supplying column is higher than the bottoms temperature of the heat receiving column. The necessary operating pressure of the columns is determined by means of flash calculations for a fixed approach temperature of 10 K, avoiding a complex economic optimization. Additional heat exchangers and heat duties are further considered to adjust the feed state of the respective column at liquid boiling conditions for the altered column pressure, as well as to compensate for any mismatch between the heat duties of the heat integrated condenser and reboiler.

Each condenser of one column can act as the heat source, while the each reboiler of another column acts as potential heat sink, and either the pressure in the heat supplying column is increased or the pressure in the heat receiving column is decreased. Therefore, four HI direct sequences (shown in Fig. 5), indirect sequences and prefractionator configurations without a thermally coupled connection between both columns are evaluated.

For the sloppy split with three columns, significantly more combinations are possible, as all three columns can be linked by means of two heat integrations that also include configurations in which one column acts as the heat receiving column for another column, while simultaneously supplying heat to the remaining column. This results in 12 heat integrated variants of the sloppy split with a single heat integration and 18 variants with two heat integrations, summing up to a total of 42 heat integrated configurations.

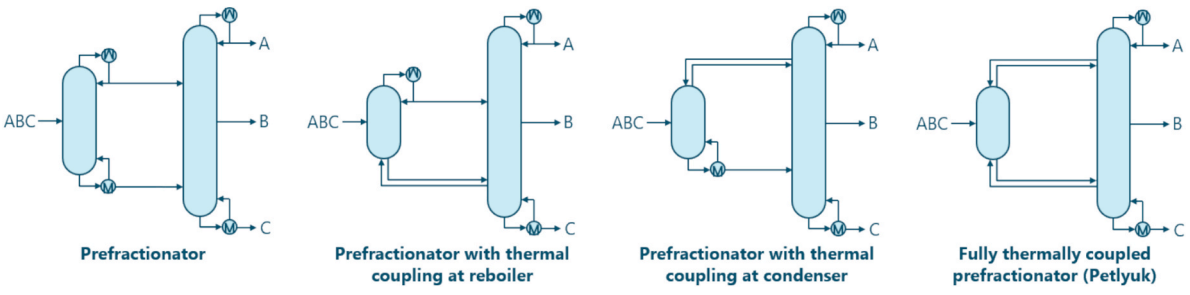

Fig. 2. All four thermally coupled variants based on the sloppy split resulting in four prefractionator configurations.

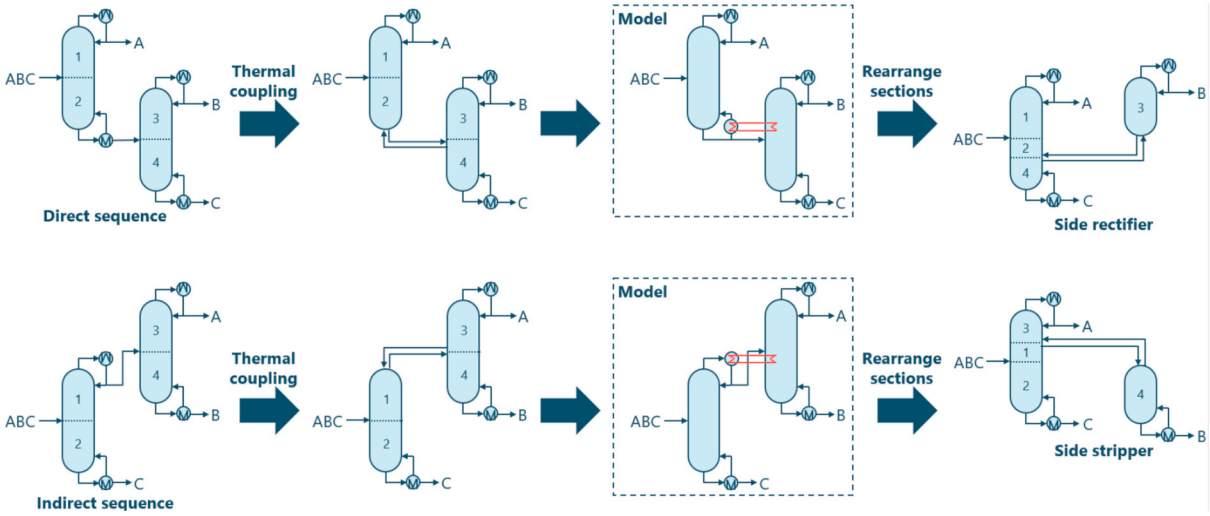

Fig. 3. Transition from direct sequence and indirect sequence to side rectifier and side stripper via thermal coupling and rearranging of column sections, with respective models.

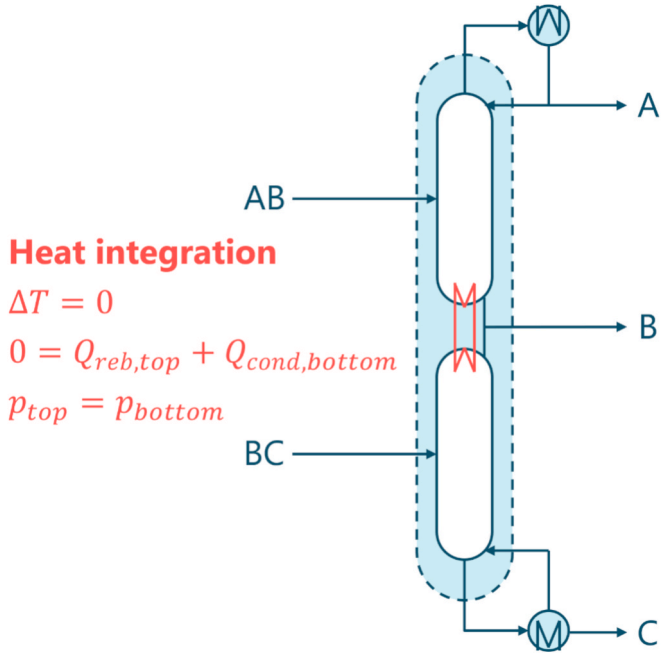

Fig. 4. Second column of prefractionator configuration modeled as two heat integrated columns.

2.1.4. Multi-effect distillation

Multi-effect distillation is a measure for heat integration for individual splits that applies direct HI between several columns contributing to the same separation, while being operated at different pressures. Direct heat integration between the different columns enables a reduced net energy requirement at the cost of an increased investment, resulting from the increased number of columns and heat exchangers. While multi-effect distillation can be conducted in different ways, either splitting the feed between different columns that conduct the same separation or having each column provide one similar product while subsequent columns process the other product of the preceding column, the current framework considers only the first option by dividing the feed stream between multiple columns. This pragmatic decision also considers that the other option does not result in sharp splits, which may temper the accuracy of the pinch-based shortcut method. Within this work, dual-effect and triple-effect distillation are considered, of which the heat receiving columns are operated at increased pressure. The working pressure is determined identically as for directly heat integrated sequences with flash calculations for an approach temperature of 10 K and the distribution of the feed stream is determined such that the rejected heat from the heat rejecting column exactly matches the heat demand of the heat receiving column. In total, 13 dual-effect and 13 triple-effect variants are evaluated for the three simple column configurations, considering dual-effect distillation for each individual column as well as any combination of columns. The three possible dual-effect variants of the direct sequence are illustrated in Fig. 6 where either the first, second or both separations are implemented as dual-effect distillation.

2.1.5. Mechanical vapor recompression

Heat integration via VRC is achieved by compressing the top vapor from one column sufficiently to raise its boiling temperature to a level suitable to provide heat for the evaporation of a bottoms stream. In this work, we focus on the VRC configuration illustrated in Fig. 7, which is consistent with other screening-related VRC studies in the literature [23,25,27,69].

The pressure after compression p_{high} is determined on the basis of flash calculations such that the saturated liquid temperature (=bubble point) of the distillate $T^{Dist}_{sat,L,p_{high}}$ is greater than the saturated vapor temperature (=dew point) of the bottom stream at the reboiler $T^{Bot}_{sat,V,p_{column}}$ by a specified approach temperature of ΔT :

$$T^{Dist}_{sat,L,p_{high}} = T^{Bot}_{sat,V,p_{column}} + \Delta T \tag{2}$$

The approach temperature can be specified in advance and is considered to be 5 K in the current investigations. If the temperature after isentropic compression, computed on the basis of specific entropy computations, is lower than the temperature of the saturated vapor at the increased pressure, the vapor from the column top with flow rate $\dot{n}_{VRC}$ is first superheated to prevent condensation in the compressor. The respective heat duty is computed on the basis of the enthalpy difference as:

$$\dot{Q}_{preheater} = \dot{n}_{VRC} \cdot \left(h_2\left(T_2^{Dist}, p_{column}\right) - h_1\left(T^{Dist}_{sat,V,p_{column}}, p_{column}\right)\right). \tag{3}$$

The electrical compressor duty is computed as

$$\dot{W}_{el} = \dot{n}_{VRC} \cdot \Delta h_{2\to 3} = \dot{n}_{VRC} \cdot \frac{h_3\left(T_3^{Dist}, p_{high}\right) - h_2\left(T_2^{Dist}, p_{column}\right)}{\eta_{mechanical}}, \tag{4}$$

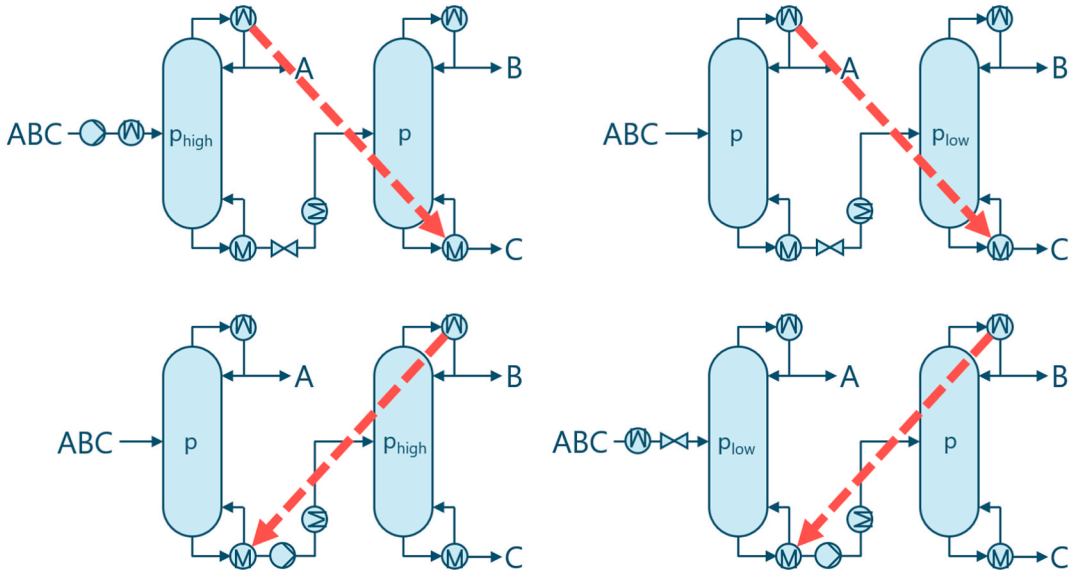

Fig. 5. All four directly heat integrated versions of the direct sequence. Dashed red arrows indicate the direction of direct heat integration. (For interpretation of the references to colour in this figure legend, the reader is referred to the web version of this article.)

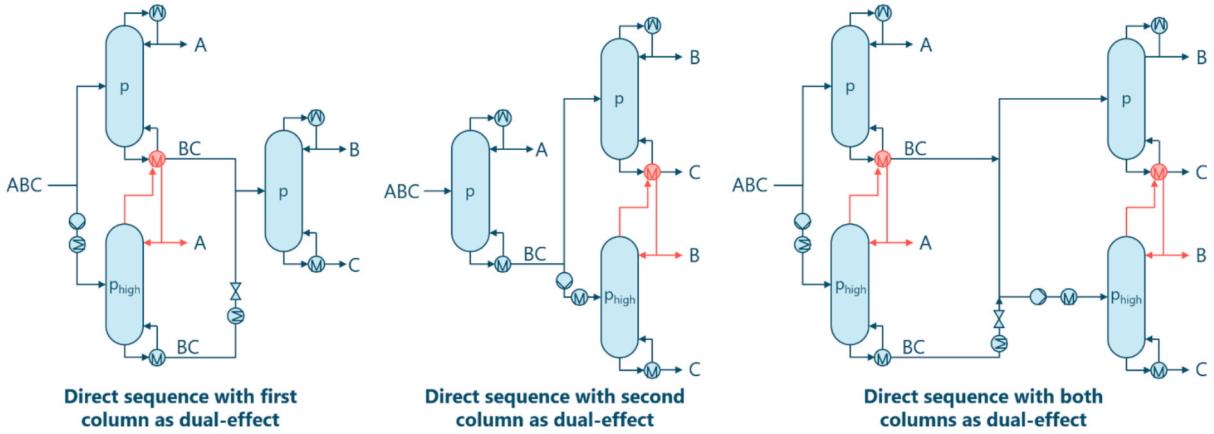

Fig. 6. All three dual-effect versions of the direct sequence, where either the first column, second column or both columns are implemented as dual-effect.

determined based on an the specific enthalpy difference for isentropic compression with an isentropic efficiency of 85 %, and mechanical efficiency of $\eta_{mechanical} = 95$ %, which is in agreement with Rix *et al.* [23], but can be adapted if needed. The amount of integrated heat is calculated as

$$\dot{Q}_{integrated} = \dot{n}_{VRC} \cdot \Delta h_{3\to4} = \dot{n}_{VRC} \cdot \left(h_4\left(T_4^{Dist}, p_{high}\right) - h_3\left(T^{Dist}_{sat,L\,p_{high}}, p_{high}\right) \right), \tag{5}$$

unless the heat for full condensation of the high-pressure vapor exceeds the required reboiler duty, in which case no additional heat is required. However, due to the lower heat of vaporization at higher pressures, in most cases the reboiler duty is not exceeded and the remaining heat is supplied externally in an auxiliary heat exchanger.

An additional condenser ensures that the reflux and distillate are saturated liquid streams.

$$\dot{Q}_{condenser} = \dot{n}_{VRC} \cdot \Delta h_{4\to5} = \dot{n}_{VRC} \cdot \left(h_5\left(T^{Dist}_{sat,L\,p_{column}}, p_{column}\right) - h_4\left(T_4^{Dist}, p_{column}\right) \right) \tag{6}$$

In the current work, VRC is considered for each combination of condenser and reboiler in any of the previously described configurations. For the direct and indirect sequence and the prefractionator configuration with 2 reboilers and condensers, six VRC configurations are evaluated. The individual links are illustrated for the direct sequence in Fig. 8. For the sloppy split with 3 reboilers and condensers a total of 33 VRC configurations are evaluated. Depending on the number of columns and level of energy-integration, different numbers of VRC configurations are evaluated, resulting in several hundred additional configurations, which include combinations of heat pumps with thermal coupling and HI.

While the current VRC configuration illustrated in Fig. 7 may not result in full electrification, a modification with an additional flash recycle, as recently proposed by Modla and Lang [70] can further improve the integration [24,71,72]. After partial condensation in the integrated reboiler, the resulting two-phase stream is split at low pressure and the vapor is recycled back into the compression cycle. This improvement has however not yet been implemented in the current framework and is a potential improvement for future work.

2.2. Minimum energy demand evaluation for individual splits

As described in the previous section, a large number of configurations are to be evaluated, potentially requiring the repeated evaluation

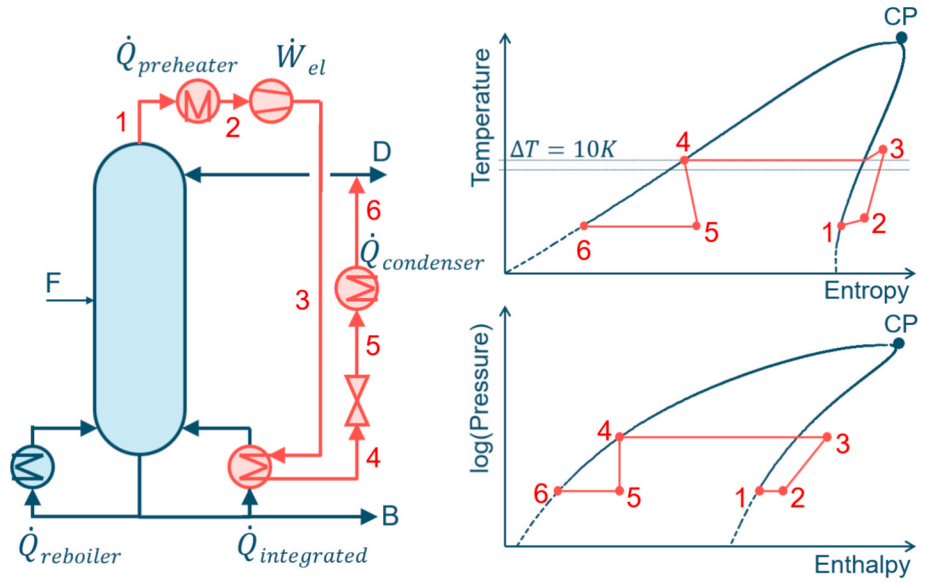

Fig. 7. Flowsheet and compression cycle diagrams of VRC for individual column.

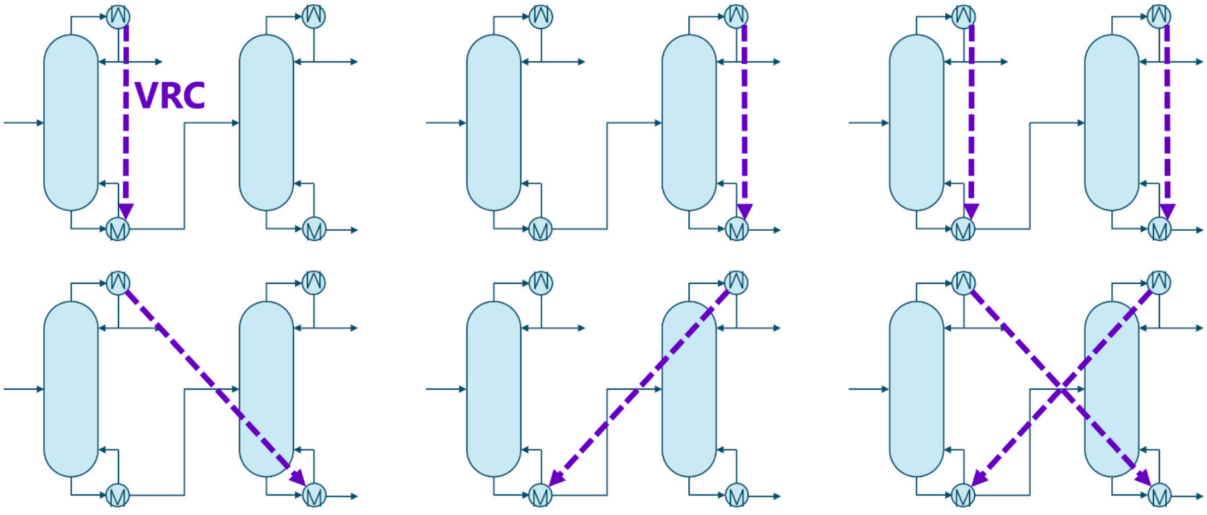

Fig. 8. All six process variants of the direct sequence with vapor recompression. Dashed purple arrows indicate the direction of transferred heat with vapor recompression. (For interpretation of the references to colour in this figure legend, the reader is referred to the web version of this article.)

of the minimum energy duty of individual splits. At the same time, simplifying assumptions for constant molar overflow and constant relative volatilities are to be avoided to enable sufficiently accurate estimates for nonideal mixtures. While rigorous simulation and optimization methods for detailed MESH models and superstructure models are available, the respective computational effort limits the application to such a large-scale screening. A number of thermodynamically sound pinch-based shortcut methods have been developed and reported in literature, which effectively reduce the computational effort, by focusing solely on individual pinch points, instead of solving the interconnected tray-to-tray models [55]. While most of the methods are not available as pre-compiled computer code, the Rectification Body Method as outlined by Bausa *et al.* [64,73] is available as part of the process synthesis software collection of AVT.SVT at RWTH Aachen University [65]. The Rectification Body Method applies to homogeneous, non-reactive mixtures with any number of components, including non-ideal systems like azeotropic mixtures, and only assumes an infinite number of equilibrium stages in order to generate linear bodies from the pinch points for the approximation of the manifolds of the potential tray-to-tray profiles in the individual column sections, which can also be used to evaluate complex columns [66]. Unlike other pinch-based shortcut methods, the Rectification Body Method determines all possible pinch points, by means of a homotopy-continuation approach, and subsequently forms the individual rectification bodies, considering further tests for a consistent entropy production as well as reachability or tangent pinches [64,74], to exclude non-physical combinations. The MED is computed based on the minimum intersection of the rectification bodies of the stripping and rectifying sections, which is assumed to enable a continuous stage-to-stage profile that renders the separation feasible.

While the Rectification Body Method can be considered as thermodynamically sound and computationally robust shortcut method, it is important to note that any pinch-based shortcut method should only be applied for suitable product specifications. Assuming a feasible separation with an infinite number of equilibrium trays requires the products to have the highest possible purity, rendering the products to either sharp splits, limited by a distillation boundary or a tangent pinch. Therefore, being able to specify sharp splits without the need for

impurities is on the one hand side a benefit of the Rectification Body Method, but also a limitation, since impurities may result inaccuracies due to vanishing pinch points. Apart from that, the linear approximation of the rectification bodies may result in inaccuracies for strongly nonlinear tray-to-tray profiles, which is however of limited relevance in most cases [64].

2.3. Optimization of operating parameters for minimum energy demand

The sloppy split and all process variants derived from it, including all prefractionator configurations and heat integrated sloppy split variants, exhibit a degree of freedom in the distribution of the intermediate product fraction of the first column. In total, 54 out of the 78 base configurations involve non-sharp splits and therefore require optimization of this internal distribution to minimize external energy demand. The distribution can be described by the ratio of flowrates

$$\psi = \frac{\dot{n}_{distillate,B,1}}{\dot{n}_{distillate,B,1} + \dot{n}_{bottom,B,1}}, 0 < \psi < 1, \tag{7}$$

between the flow rate of the distributed fraction B as displayed in Fig. 9 (left) in the distillate $\dot{n}_{distillate,B,1}$ and in the bottom stream $\dot{n}_{bottom,B,1}$ of the first column: The distribution is limited between 0 and 1 and can be freely chosen without impacting the split feasibility, but strongly affects the flowrate and composition of the first column's product streams, as well as the minimum energy demand of the entire configuration.

Consider the distribution of the intermediate fraction B for the prefractionator configuration for which the entire fraction A is in the distillate and the entire fraction C is in the bottom stream of the prefractionator. Depending on the distribution of B, different minimum energy duties are computed for the separation of an equimolar mixture of benzene, toluene and p–xylene into pure products at 1 bar, with a minimum energy demand for the prefractionator configuration at a distribution factor of 0.3 as illustrated in Fig. 9 (right). Note that the flat optimum for the fully thermally coupled prefractionator represents the optimality region that can also be analyzed by the Vmin diagram presented by Halvorsen and Skogestad [75] considering that a rigorous evaluation of the VLE computations and enthalpy balances is applied in the derivation.

Therefore, for such configurations an optimization of the distribution factor is performed to identify the flowrates and compositions of internal streams which minimize the overall energy demand of the entire configuration and not just that of the individual columns. The optimization problem is formulated as $\min_{\psi} f(\psi) = External\ Eergy\ Demand$, *with* $0 < \psi < 1$, and solved with the MATLAB solver-function 'fmincon' using the gradient based interior-point method with a relative abort tolerance of 10^{-3} for the step size with each iteration. Preliminary studies have shown that the minimum is reliably found when starting from an initial value $\psi^{(0)} = 0.5$. Since the Rectification Body Method itself operates with a bisection and consequently does not provide gradient information, gradients are approximated using conjugate gradients with a step size of 10^{-4}, while the Hessian is estimated via the BFGS method.

For multi-effect distillation the individual distribution of the feed is determined such that the condenser and reboiler duties of adjacent columns match, without necessitating such an optimization. While each individual configuration without VRC is consequently optimized to represent the overall MED, VRC is implemented for each individual configuration as a post-processing step. In case a VRC configuration would benefit from a sub-optimal design of the configuration without VRC, this would not be covered in the current screening. This sequential approach reduces computational demand significantly, as the many VRC variants would otherwise require individual optimization requiring extensive resources. While this can be considered as some limitation, we do not expect considerable improvements.

2.4. Economic evaluations

Although energy demand can serve as a rough estimation of process costs [66] since higher energy requirements often indicate more challenging separations that necessitate additional stages, increased column diameters, and larger heat exchanger surfaces [60], a rigorous cost estimation has several benefits. It particularly accounts for the number of columns and heat exchangers, the significant investment in compressors, and available utilities at specific conditions and prices. To provide a more comprehensive picture, the total annual cost

$$\mathrm{TAC} = C_{op} + CCF \cdot C_{inv,total}, \tag{8}$$

configuration with a capital charge factor

$$\mathrm{CCF} = \frac{i \cdot (1+i)^t}{(1+i)^t - 1} \tag{9}$$

based on a given depreciation period t in years and specific interest rate i. For the following studies, with the exception of Section 3.2.3, an interest rate of 6 % and a depreciation period of 10 years are considered. The calculation of investment cost $C_{inv,total}$ and annual operating cost C_{op} is described in the following subsections.

2.4.1. Operating cost calculation

The annual operating cost

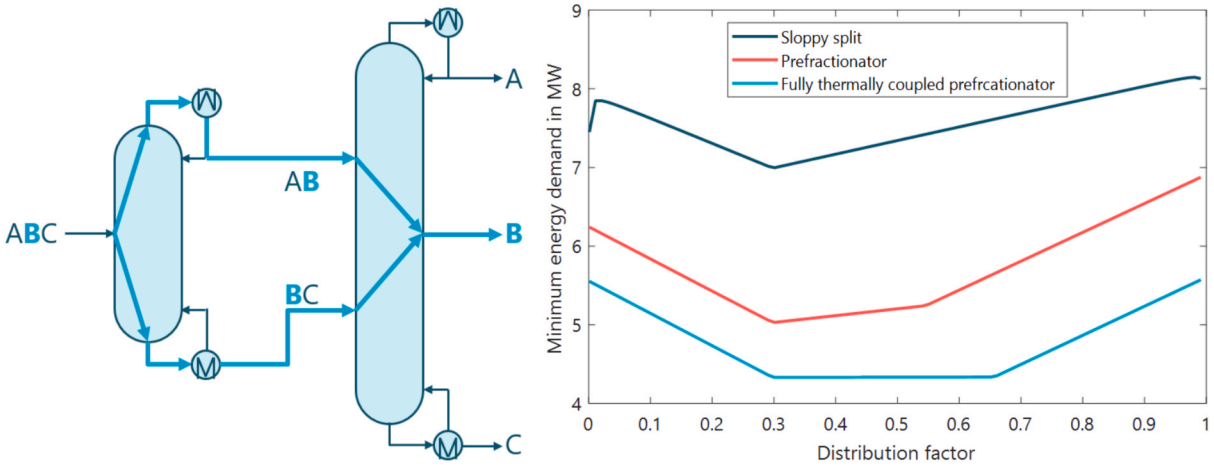

Fig. 9. Degree of freedom in the distribution of fraction B for a prefractionator configuration (left) and influence of distribution factor on minimum energy demand for separation of equimolar benzene – toluene – p-xylene mixture into pure products (100 mol/s, 1 bar, NRTL, Redlich-Kwong).

$$C_{Op} = t_a \cdot \sum C_{Utility} \cdot Q_{Utility} \tag{10}$$

depends on the annual operating time t_a, which is assumed as 8000 h. For the sake of the current case studies in Section 3 the utility network given in Table 1, which is based on Turton *et al.* [76, p. 231], is considered, but these parameters can easily be modified, as illustrated in Section 3.2. For all specified cold utilities, a temperature increase of 10 K in the heat exchangers is considered, while total condensation of steam is assumed. For all heat exchangers with external utilities, the cheapest feasible utility is chosen automatically. For the following case studies, a minimum temperature difference of 10 K needs to be provided.

2.4.2. Capital cost calculation with Guthrie's module factor method

Capital costs estimates are derived from the shortcut results and reflect the varying numbers and sizes of individual process equipment. For each column the difficulty of the separation and the computed vapor flow rates are considered, while the cost of heat exchangers are affected by the specific energy integration scheme, with the according number of required heat exchangers and temperature levels, resulting in different heat exchanger areas. For heat pumps the substantial investment required for compressors must be considered for a comprehensive evaluation.

The capital cost of each piece of equipment is estimated using Guthrie's module factor method with the correlations by Biegler *et al.* [63], extending the original approach by incorporating additional module factors and inflation correction factors [77, pp. 132–133]. This method is well suited for conceptual design and provides an accuracy of approximately ±30 % [78, pp. 306–307] by considering only the major pieces of equipment: Column shell, tray stacks or packings (including liquid distributors, liquid collectors and support grid) depending on the utilized type of internals, heat exchangers and compressors, using update factors to account for shipment, insurance and engineering.

The base capital cost

$$C_{Cap,Base,Equip} = C_{0,Equip} \cdot \left(\frac{Q_{Equip}}{Q_{0,Equip}} \right)^{\gamma} \tag{11}$$

of any piece of equipment is calculated based on a reference cost $C_{0,Equip}$ with standard capacity $Q_{0,Equip}$. An individual exponent γ is assigned to each piece of equipment to account for the economy of scale, while Q_{Equip} refers to its actual capacity.

Once the equipment capacity is determined (as detailed in the next section), the base capital costs are adjusted using size-based module factors *MF* to account for installation cost and correction factors *CF* that reflect differences in material, design, and operating conditions These adjustments are then combined with an inflation correction factor *UF* to arrive at the final estimated capital cost. The total capital cost $C_{Cap,total}$ is obtained by summing the bare module capital cost

$$BMC = UF \cdot C_{Cap,Base,Equip} \cdot \left(MF - 1 + \sum CF \right) \tag{12}$$

for each piece of equipment [77, p. 135]. The inflation factor is determined by dividing the present cost index by the cost index corresponding to the year of the provided cost data, with the Chemical Engineering Plant Cost Index (CEPCI) of June 2024 used as the present cost index. A more detailed overview of the cost calculation including design choices and correction factors, based on Biegler [77] is provided in the Supporting Material.

Table 1
Utilities and their prices used for the cost calculation [76, p. 231].

Utility	Utility price [$/GJ]	Utility price [$/kWh]
Cooling water (30 °C → 40 °C)	0.354	0.001
Refrigerated water (5 °C → 15 °C)	4.43	0.016
Cooling brine (−20 °C → -10 °C)	7.98	0.029
Cooling brine (−50 °C → −40 °C)	13.11	0.047
Low pressure steam (6 bar, 160 °C)	14.05	0.051
Medium pressure steam (11 bar, 184 °C)	14.83	0.053
High pressure steam (42 bar, 254 °C)	17.70	0.064
Electricity	16.80	0.060

2.4.3. Equipment size estimation

For the column pressure vessel, the relevant design capacities are its height and diameter. For the column internals, the key capacities include the column diameter as well as the effective height of the tray stack or packing section, which is determined by the required number of (equivalent) equilibrium stages. For heat exchangers, the heat transfer area serves as relevant capacity while for compressors it is defined by the electrical duty.

Because the Rectification Body Method determines the MED corresponding to a minimum reflux ratio r_{min} for a given separation under the assumption of an infinite number of stages, the actual number of stages N_{actual} of each column has to be estimated for calculating the column height. Usually, the Fenske equation (see eq. (1)) is used to determine an estimate for the minimum number of equilibrium stages N_{min} for a separation at total reflux. This equations does however require the assumption of constant relative volitivity [38]. The Winn equation [61]

$$N_{min} = \frac{ln\left(\frac{x_{LK,top}}{x_{LK,bottom}} \cdot \left(\frac{x_{HK,bottom}}{x_{HK,top}} \right)^{b} \right)}{ln(\beta)} \tag{13}$$

provides a more accurate estimation that builds on the compositions (x) and equilibrium constants (K) of the heavy (*HK*) and light key (*LK*) components at the top and bottom end of the column to determine the factor

$$\beta = \frac{K_{LK,top}}{K_{HK,top}^{\ b}}, \tag{14}$$

with

$$b = \frac{ln\left(\frac{K_{LK,top}}{K_{LK,bottom}}\right)}{ln\left(\frac{K_{HK,top}}{K_{HK,bottom}}\right)}. \tag{15}$$

For conventional columns, the Winn equation is applied only once for the entire column, but for side stream columns, such as the second column of the prefractionator configuration, the minimum number of equilibrium stages is calculated separately for the section above and below the side stream and the sum used as the minimum number of equilibrium stages for the entire column.

Both the light and the heavy key component are identified automatically as the heaviest component that has a higher composition at the top than at the bottom (*HK*) and as the lightest component that has a lower composition at the top than at the bottom (*LK*). While the Winn equation does not assume constant relative volatilities throughout the column, it still builds on the simplifying assumption of a linear volatility change throughout the column w.r.t. the key components. Consequently, the resulting number of stages is still an estimate that may be quite inaccurate for strongly non-ideal mixtures. However, the Winn equation remains the preferred option for shortcut-based estimations, which avoid the computational burden of detailed stage-to-stage calculations.

To ensure a finite minimum number of equilibrium stages for columns specified to perform sharp separations, an artificial impurity is introduced to the key components when they exceed a certain purity level. Without this adjustment, perfectly sharp separations would theoretically require an infinite number of stages. A reduced product purity of 99.99 mol% is considered for the computation of the minimum number of equilibrium stages for pure component products.

Once the minimum number of equilibrium stages is determined, the number of equilibrium stages N is estimated using the Gilliland correlation

$$N = \frac{N_{min} + 0.75 \cdot \left(1 - \frac{r - r_{min}}{r+1}\right)^{0.5688}}{1 - 0.75 \cdot \left(1 - \frac{r - r_{min}}{r+1}\right)^{0.5688}} \tag{16}$$

with an approximation for actual reflux ratio $r = r_{min} \cdot 1.2$ based on the minimum reflux ratio determined beforehand with the MED as a practical compromise between reflux ratio and required number of stages [79]. For tray columns, the number of trays is finally obtained as the next highest integer while also considering a possible tray efficiency μ_{tray}. The tray stack height $H_{traystack}$ is calculated according to Douglas [79, p. 453] based on actual number of stages and tray spacing h_{tray}, which also determines the critical flooding factor F_{crit}. The pressure vessel height

$$H_{column,trays} = 1.15 \cdot H_{traystack} = 1.15 \cdot \left\lceil N \cdot \mu_{tray} \right\rceil \cdot h_{tray} \tag{17}$$

is the tray stack height with an additional 15 % for the sump, overhead space, manholes, demister, etc..

For packed columns, the type of employed packing determines the critical flooding factor and the overall column height

$$H_{column,packed} = HETP \cdot N + D + 1m \cdot n_{beds} + 1m \cdot (n_{beds} - 1) + 0.5m \cdot (n_{beds} + 1) \tag{18}$$

is derived from the height equivalent of a theoretical plate *HETP*, reflecting a specific internal, and the number of equilibrium stages required. Further details on the equipment sizing and cost estimation are described in Section S3 of the Supporting Information.

3. Case studies

To illustrate the capabilities of the algorithmic framework, two case studies are presented. The first case study showcases illustrates the screening of the most promising processes for a given ternary separation problem, also considering uncertain process conditions and thermodynamics. The second case study highlights the applicability for nonideal multicomponent mixtures and analyses the sensitivity of the results w.r.t. utility costs and the capital charge factor considering the different energy-integration methods.

All calculations assume saturated liquid feeds with a flow rate of 10 mol/s, and unless stated otherwise, the NRTL model is applied as G^E-models to account for the nonideality of the liquid phase and the Redlich-Kwong equation of state is used to account for the nonideality of the vapor phase at high pressures. The extended Antoine equation is used to compute the pure component vapor pressure, while DIPPR correlations are applied for the computation of specific heat capacities and heat of vaporization. The utilized thermodynamic property models and respective property parameters are presented in Section S1 and S2 of the Supporting Information. For separations at or above atmospheric conditions, trays are employed as column internals, whereas the use of structured packings is considered for columns operating under vacuum conditions to ensure negligible pressure drop, aligning with the model assumptions. All computations are performed on a PC with an Intel i7-8700 CPU using MATLAB R2024b through computation on 6 parallel workers making use of the Parallel Computing Toolbox.

3.1. Separation of a ternary mixture of benzene, toluene and p-xylene

A feed consisting of an equimolar mixture of the well-studied mixture of benzene, toluene and p-xylene [80–84] is separated into pure products at a reference pressure of 1 atm. The screening and optimization of a total of 775 process options effectively requires ~200 s of wall clock time. Based on the temperature levels of the available utilities 28 configurations with larger pressure variations are discarded. Considering a lower pressure limit of 50 mbar to avoid deep vacuum operation, a maximum compression ratio of 7 and a maximum compressor discharge temperature of 150 °C for VRC configuration many of the VRC variants are excluded, which is rooted in the boiling point of p-xylene (138 °C) that is very close to the discharge temperature limit. After applying these practical limits, 222 variants are still feasible and further evaluated in the following subsections.

3.1.1. Energetic and economic performance

The best 20 processes regarding TAC and net MED are highlighted in Figs. 10 and 11, summarizing their distribution for practically feasible sequences. All sequences requiring electricity use VRC, effectively limiting operating costs, but require significant investment for the compressors.

The nine sequences with the lowest net energy demand utilize VRC, in one case in conjunction with multi-effect distillation and in another in combination with direct HI. The lowest net energy demand (MED = 161 kW) is determined for a direct sequence with VRC for each column (DS-VRC), ranking #10 regarding TAC (308 k$). The configurations ranking #10 and #11 apply only direct HI with almost identical energy demands of 237 kW, however requiring over 45 % more external energy than the DS-VRC. The first of these is derived from the prefractionator with HI from the first to the second column (PF-HI12) which also has the lowest TAC (249 k$) and the other is a variant of the sloppy split with two HI links (SLOPPY-HI132) ranking #3 regarding TAC (269 k$).

Looking at the economic ranking in Fig. 12, the top nine sequences all employ direct HI. Four of these configurations are based on the sloppy split with three columns and two directly heat integrated links, while two other configurations are sloppy split sequences with only one direct HI link and another VRC connection. This highlights that despite the use of three columns, heat integrated configurations based on the sloppy split appear economically attractive despite the large number of equipment, due to the reduced operational cost. Yet, it needs to be stressed, that these configurations are highly integrated and potentially complex to operate. The two configurations with the lowest TAC are a heat integrated prefractionator and direct sequence, which have an almost equivalent TAC of 250 k$. The direct sequence with HI from the first to the second column does however only rank #30 regarding MED (296 kW), highlighting the difference in the performance metrics.

The direct sequence is the best performing simple sequence, which ranks only #218, almost at the end of the feasible, options, regarding MED (625 kW) and half-way at #113 for TAC (389 k$). The best energy-integrated sequences, illustrated in Fig. 12, thus save around 74 % net energy demand and 36 % TAC respectively. Another interesting result is the ranking of the fully thermally coupled DWC, which as to be expected is the best performing thermally coupled sequence without further HI. It ranks only #129 regarding net MED (433 kW), but due to the possible equipment integration and respective capital cost savings ranks #16 regarding TAC (314 k$). Interestingly, the DWC offers net energy savings of 31 % compared to the direct sequence, aligning well with reported literature values [85], but actually has almost identical capital costs despite only using one column shell. While the combined height of both columns of the direct sequence is similar to the height of the combined column shell of the DWC, the diameter of the DWC is larger, because the entire column is operated at the vapor demand of the most difficult separation. Compared to the (thermodynamically equivalent) fully thermally coupled prefractionator with two column shells, the DWC's capital costs are however reduced by 9 %.

3.1.2. The influence of pressure on cooling utilities and TAC

Interestingly, four of the 20 lowest TAC configurations require refrigerated water due to low condenser temperatures of columns operated at vacuum to facilitate direct HI, resulting in high cooling costs. This is also the reason for the increased cooling cost of the PF-HI12,

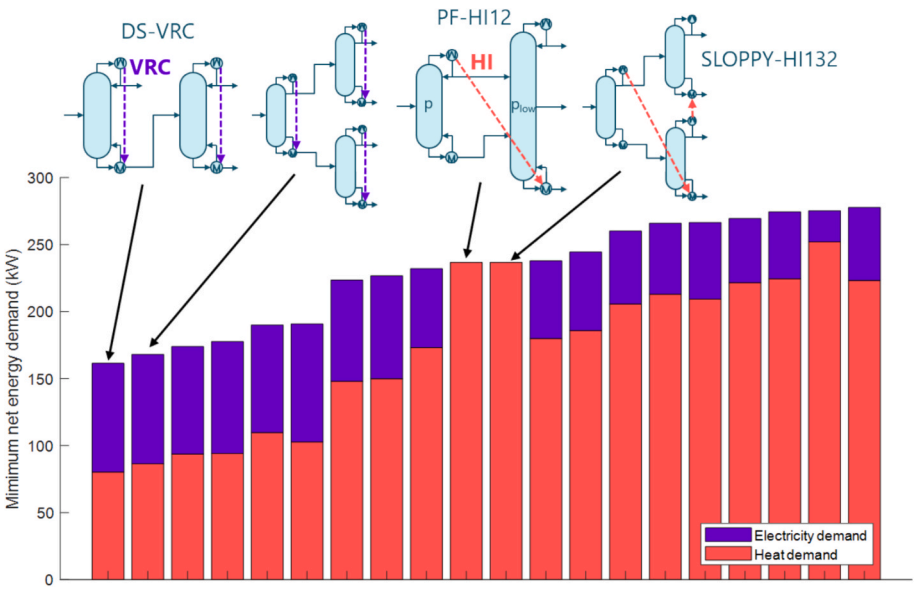

Fig. 10. Distribution of MED for 20 practically feasible sequences with lowest net MED at base pressure of 1 atm.

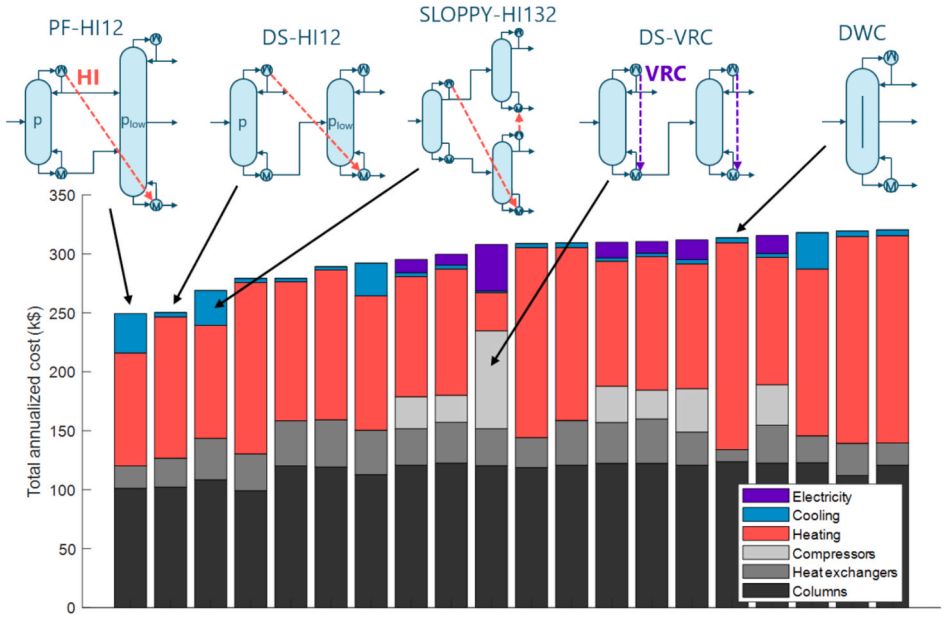

Fig. 11. Distribution of TAC for 20 practically feasible sequences with lowest TAC at base pressure of 1 atm.

which provides anyway the lowest TAC. It has a condenser temperature of 25.6 °C at the second column operated at 130 mbar. To investigate if one of the five configurations with the lowest TAC at given conditions yields economic benefits for an increased reference pressure, a sensitivity analysis w.r.t. to the reference pressure is performed, and the results are shown in Fig. 13.

It is apparent that the reference pressure has a complicated effect on the TAC, resulting from changes in utilities, as well as size-based module factors, choice of column internals, as well as the direct influence on volatilities and heat of vaporization of the components. These aspects also make an optimization for the TAC quite challenging, as especially the discrete decisions for utility and material changes introduce step changes that would require proper smoothing to facilitate a mathematical optimization. Therefore, the capabilities of the presented screening tool to perform such a sensitivity analysis in just a few minutes provides much valuable information to identify the most interesting configurations and define a properly formulated optimization problem for a more detailed design.

The results indicate that PF-HI12 has the lowest TAC for all reference pressures up to ~4.7 bar, although from ~2.9 bar on for the PF-HI12 and from ~3.2 bar on for the DS-HI12, a more expensive high temperature steam is required. The SLOPPY-HI132 outperforms the DS-HI12 beyond about 2.2 bar and even has the lowest TAC for two of the considered pressures of ~4.8 bar. The lowest overall TAC of 222 k$ is achieved by the PF-HI12 for a reference pressure of 2.23 bar. At this pressure, it also provides the lowest net MED (252 kW), similar to that of the SLOPPY-HI132 with two direct HI links. This is however significantly larger than the net energy demand achieved by VRC-assisted configurations at a base pressure of 1 atm (cf. Fig. 11), which are however infeasible due to the increased discharge temperature at the increased reference pressure.

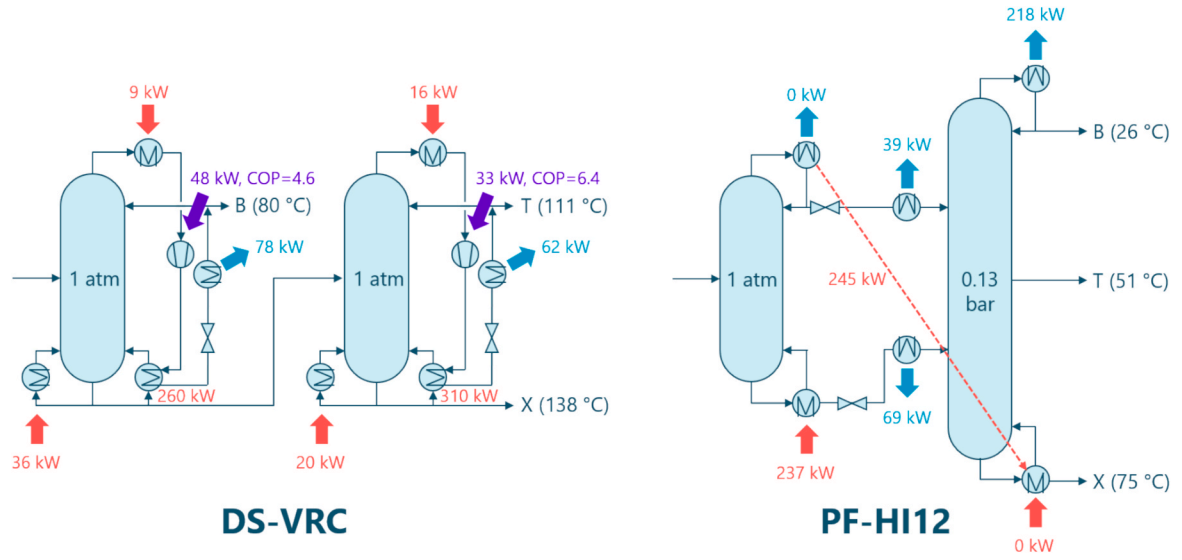

Fig. 12. Flowsheets of configurations with lowest net MED (DS-VRC, left) and lowest TAC (PF-HI12, right).

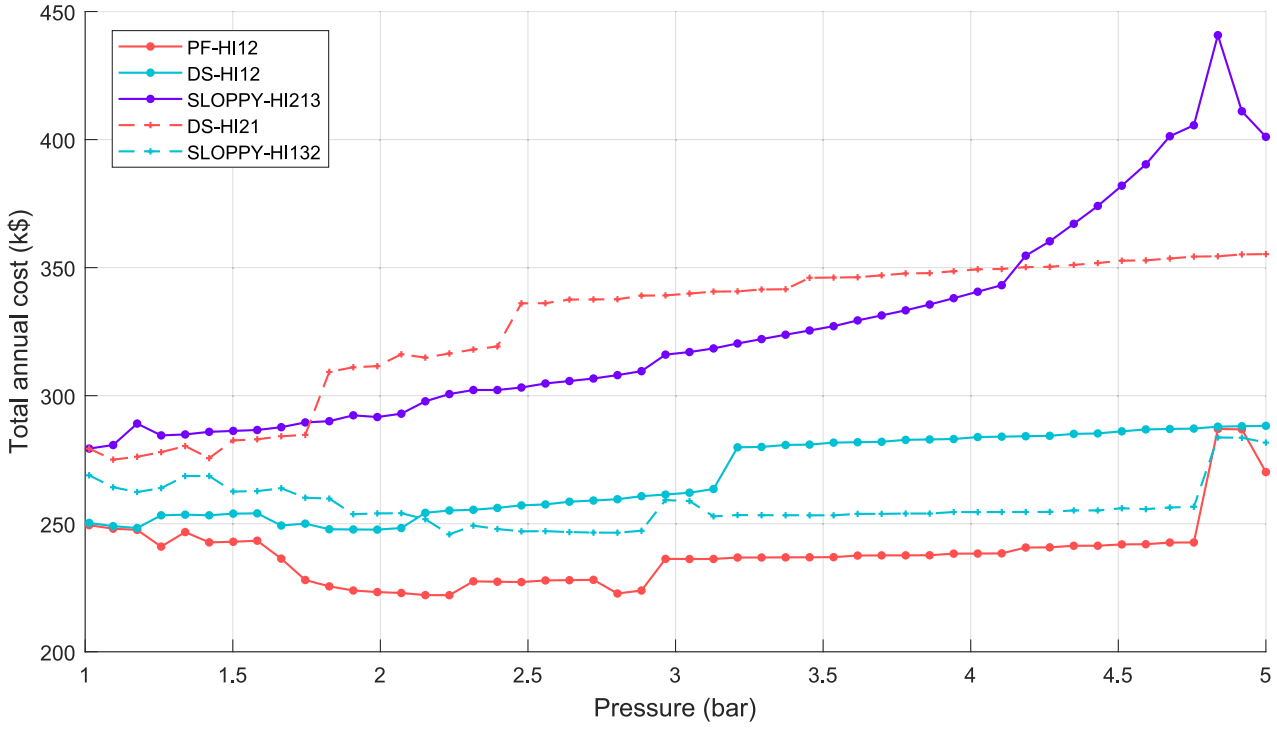

Fig. 13. Sensitivity of TAC over pressures for five lowest-TAC configurations.

3.1.3. Multi-criteria evaluation of investment and operating costs

As investment cost and operating costs are competing objectives, it is interesting to analyze the particular distribution, as illustrated in Fig. 14, which includes all practically feasible sequences at reference pressures of 1 atm and 2.23 bar. On closer inspection, many configurations, as indicated for the highlighted options, benefit from reduced capital investment at the higher pressure due to smaller column diameters resulting from lower volumetric vapor flow rates. As previously stated, the PF-HI12 and DS-HI12 provide the best economic performance and can be considered pareto-optimal, with the PF-HI12 having the lowest operating costs for the chosen depreciation period and interest rate, while the DS–HI12 having the lowest investment cost, but a somewhat higher operating cost. Obviously, the DWC configuration is considerably dominated in both operating and investment cost by these configurations for the specific economic evaluations independent of the reference pressure level. At a reference pressure of 1 atm, several VRC configurations offer even lower energy demand and operating costs, but require a considerably larger investment, due to the expensive compressor. The DS-VRC is nevertheless a pareto-optimal solution at this reference pressure and it would become more attractive in case the huge investment would become smaller due to development of less expensive compressors. As mentioned before, this configuration becomes infeasible for an increased reference pressure. These results highlight the benefit of such a multi-criteria evaluation, which is most valuable when the investment costs vary significantly between different configurations.

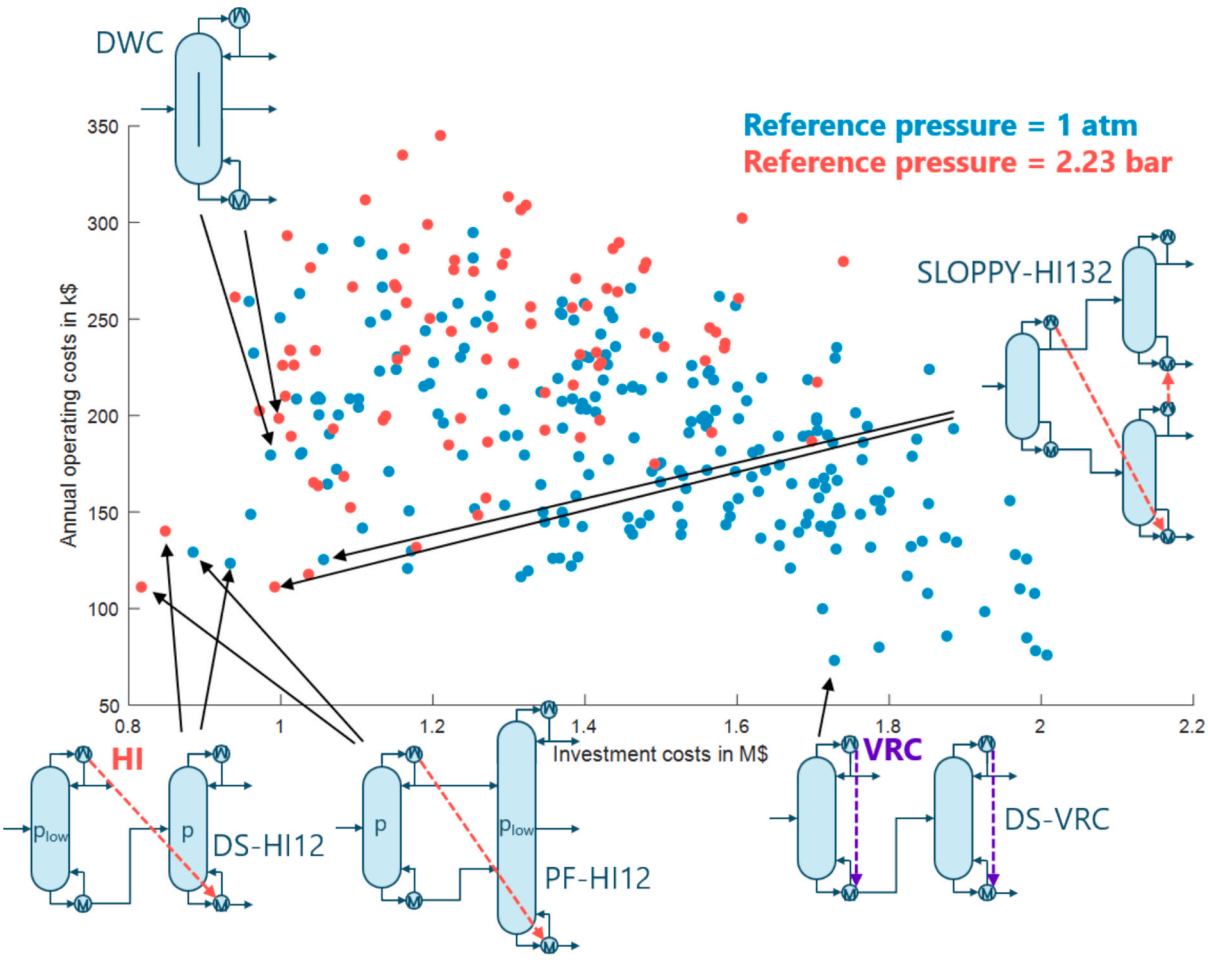

Fig. 14. Trade-off between operating costs and investment costs for practically feasible sequences.

3.1.4. Sensitivity of net MED and TAC to uncertain process conditions and thermodynamics

Given the computational efficiency of the evaluations, different parameter combinations can be tested and as such the sensitivity of these results to uncertainties in process specifications and thermodynamic models can be tested. A multi-scenario evaluation is performed in this study, for which the feed flow rate was varied by ±2 %, seven different feed compositions were tested with component-wise disturbances of ±2 %, and the operating pressure was adjusted from 2.23 bar by ±10 mbar and ±20 mbar. Additionally, three

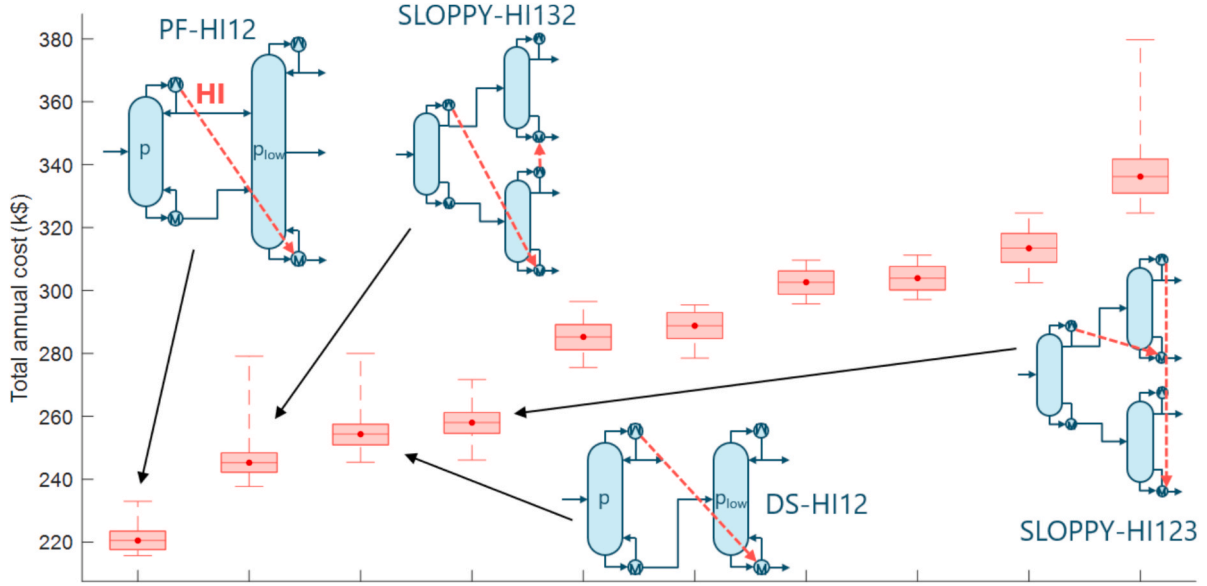

Fig. 15. Results of uncertainty investigation for 10 selected configurations, sorted by median value.

thermodynamic models (NRTL, Wilson, and UNIQUAC) were considered. In total, 315 thermodynamic scenarios are evaluated for each of the ten configurations with the lowest TAC at 2.23 bar, all within an hour of wall clock time.

The uncertainty investigation results are presented in Fig. 15 in the form of boxplots, here each box represents the distribution of TAC values across all tested scenarios for a given configuration. The line inside the box is the median TAC, while the top and bottom edges mark the 75th and 25th percentiles, capturing the middle 50 % of the results. The whiskers extend to show the remaining top and bottom 25 %, illustrating the full range of TAC values observed for each configuration. When compared to the single scenario calculation at 2.23 bar, the order of configurations by median TAC remained essentially unchanged, with the only exception being a swap between the configurations in positions 5 and 6. The PF-HI12 exhibits TAC variations of +5.7 % and −2.2 % relative to its median value, accompanied by energy fluctuations of +5.5 % and −3.4 % around a median net MED of 253 kW. In contrast, the SLOPPY-HI132 with second lowest median TAC is much more sensitive to changing conditions, with TAC fluctuations of +13.8 % and −3.1 % and energy variations of +27.4 % and −3.6 % around a median net MED of 254 kW. Yet it is important to note that even in its worst-performing scenario, PF-HI12 maintains a slightly lower TAC than any other configuration in their respective best-performing scenarios, indicating that it is a robust design choice for the given separation problem.

3.1.5. Comparison with rigorous simulation in Aspen plus

While the validity of the Rectification Body Method computations has been demonstrated in the original publications of Bausa *et al.* [64], von Watzdorf *et al.* [66] and Kraemer *et al.* [54], the accuracy of the shortcut-based evaluation is further elucidated for the well-performing PF-HI12 sequence, for which a rigorous simulation with Aspen Plus was conducted for the same separation task of an equimolar liquid boiling feed of benzene, toluene and p-xylene. The RadFrac column model with thermosyphon reboilers was employed for both columns. NRTL-RK is used as the property calculation method. The pressure of the first column (34 stages) is 2.23 bar and 0.37 bar for the second column (91 stages). The number of equilibrium stages for each column was taken directly from the shortcut-based estimation. The minimum reboiler duties as determined by the Rectification Body Method were applied, along with corresponding feed preconditioning duties, and the distillate and side-draw flow rates were specified according to the obtained shortcut flow rates.

The product purities obtained from the simulation are shown in Table 2. All components are recovered with purities of 99 mol% or higher, confirming that the shortcut-based design is thermodynamically feasible and provides an accurate estimate for process synthesis.

3.2. Separation of a quaternary mixture of acetone, chloroform, benzene and toluene

In this second case study, an equimolar quaternary feed stream is to be separated in a mixed product stream of acetone and chloroform and two pure product streams of benzene and toluene. Although the mixture forms a binary azeotrope between acetone and chloroform, resulting in a distillation boundary, the separation remains feasible by distillation because these two components are enriched together in the lightest product fraction. The subsequent analysis focusses on the economic performance, specifically analyzing the influence of utility prices and the CCF on the benefits of VRC-assisted processes and the specific process selection.

Table 2
Product purities obtained in simulation with Aspen Plus RadFrac models for second column of PF-HI12.

	Distillate	Side draw	Bottom product
Benzene [mol%]	0	99.66	0.34
Toluene [mol%]	0.63	0.34	99.02
p-Xylene [mol%]	99.37	0	0.63

For this separation, 785 different process variants are screened in just a few minutes of wall clock time. The different number of configurations compared to the previous study results from the fact, that depending on the separation, HI configurations may require differed trim heat exchangers. While a configuration may require a trim reboiler for a particular separation, it may require a trim condenser for another separation, enabling other VRC combinations. Considering the same practical limitations on operating pressures, temperature limits and maximum compression ratio, as for the previous case study, 313 different process variants remain feasible. The additional 50 %, compared to the previous case study, are primarily VRC-assisted configurations which maintain the upper temperature limits for the compression due to the lower boiling point of the highest boiling component toluene (110.6 °C at ambient pressure), which is almost 30 K lower compared to 138.4 °C of p-xylene in the previous study.

3.2.1. Minimum energy demand and economic performance

Similar to the previous case study, VRC-assisted processes dominate w.r.t. the net MED with 95 out of the best 100 configurations, given that less VRC variants are excluded due to practical constraints. The first 44 configurations with the lowest net MED are entirely VRC-assisted configurations. The remaining five variants in the top 100 are four multi-effect distillation processes and a sloppy split with two direct HI links. An exemplary overview of the best performing configurations and some variants for further comparison is listed in Table 3.

The lowest net MED of 166 kW is realized by a sloppy split with VRC for each individual column (SLOPPY-VRC), closely followed by the direct sequence with VRC for each column (DS-VRC) requiring 185 kW (+11 %). While the SS-VRC also ranks #13 in terms of TAC (647 k$), the DS-VRC has 4 % higher TAC as it requires more electricity and despite only requiring two columns, their combined height is similar to the combined column height of the SS-VRC, which however has lower column diameter on average.

The next lowest net MED is realized by the Petlyuk sequence with VRC (Petlyuk-VRC) and the equivalent DWC configuration with VRC (DWC-VRC), both requiring 190 kW. Both configurations exploit the combined savings of full thermal coupling with an additional heat pump, which in this case results in the lowest overall TAC of 549 k$ for the DWC-VRC configuration. This configuration is however only slightly more expensive than the indirect sequence with HI from the second column operated at an increased pressure to the first column (IS-HI21), which comes at a TAC of 500 k$ (+10 %) and the DS-HI12 with pressure increase in the first column at TAC of 515 k$ (+7%). Consequently, direct HI of the simple sequences comes at TAC comparable to the VRC-assisted DS and DWC, but their net MED is more than three times larger. Interestingly, despite the high costs of the compressors, 14 of the 20 configurations with the lowest TAC utilize VRC.

The importance of energy integration is easily recognized from the comparison of the best performing configurations with the direct

Table 3
Overview of results from the MED and economic evaluation of the initial screening for the separation of the equimolar acetone, chloroform, benzene, toluene mixture into three product streams, for the base case scenario.

# MED	MED (kW)	# TAC	TAC (k€/a)	Configuration
1	166	13	647	SLOPPY-VRC
2	185	22	674	DS-VRC
3	190	46	703	Petlyuk-VRC
4	190	6	549	DWC-VRC
45	399	45	702	DS-triple-effect
108	588	1	500	IS-HI21
122	638	2	515	DS-HI12
251	971	174	865	DS

sequence, which is the simple sequence with the lowest net MED of 971 kW (#251) and TAC of 865 k$ (#174). The best performing configurations thus offer more than 80 % savings in terms of net MED and more than 45 % lower TAC. With the exception of the SLOPPY-VRC, which provides a recognizable improvement in net MED at decreased TAC over the DS-VRC, more complex configurations with multiple columns and energy integration links do not offer any benefits in terms of MED, while being more expensive and complex to operate. Other configurations, such as the multi-effect direct sequence with three effects per separation (DS-triple-effect) only ranks #45 regarding both MED (399 kW) and TAC (702 k$).

3.2.2. *The influence of utility prices*

While VRC typically yields the largest energy savings, its economic viability strongly depends on the electricity prices in relation to steam costs. The utilized utility prices in Table 1 consider a relatively low electricity price compared to steam costs. The considered price per unit of electrical energy even lies below the price of the highest temperature steam in this evaluation, which is not unrealistic for high shares of renewable energy, but todays industrial companies often face higher electricity costs. In Germany, Europe's largest economy with a large chemical industry, the industrial electricity prices ranged from 0.06 to 0.18 €/kWh between 1998 and 2020, spiking to 0.43 €/kWh in 2022 [86], while natural gas as an indicator for heat prices were comparably low and stable between 2008 and 2020 ranging from 0.03 to 0.04 €/kWh spiking to 0.08 €/kWh in 2023 [87]. Consequently, electricity-to-heat price ratios of ~3–5 were maintained for most years.

Given the importance of the utility prices, the fluctuations in recent years and varying expectations owed to the development of renewable energy sources providing electricity as primal form of energy, it is crucial to evaluate the performance of the configurations w.r.t. varying price scenarios. Thereby, it can be analyzed under which scenarios VRC-assisted processes that require electrical power for compression are sufficiently economically attractive relative to more conventional HI options. Based on the results of the base case scenario reported in the preceding section the SLOPPY-VRC and DWC-VRC configurations are compared with the DS-HI12 and IS-HI21 configurations, as these were economically most attractive. The HI and VRC configurations show

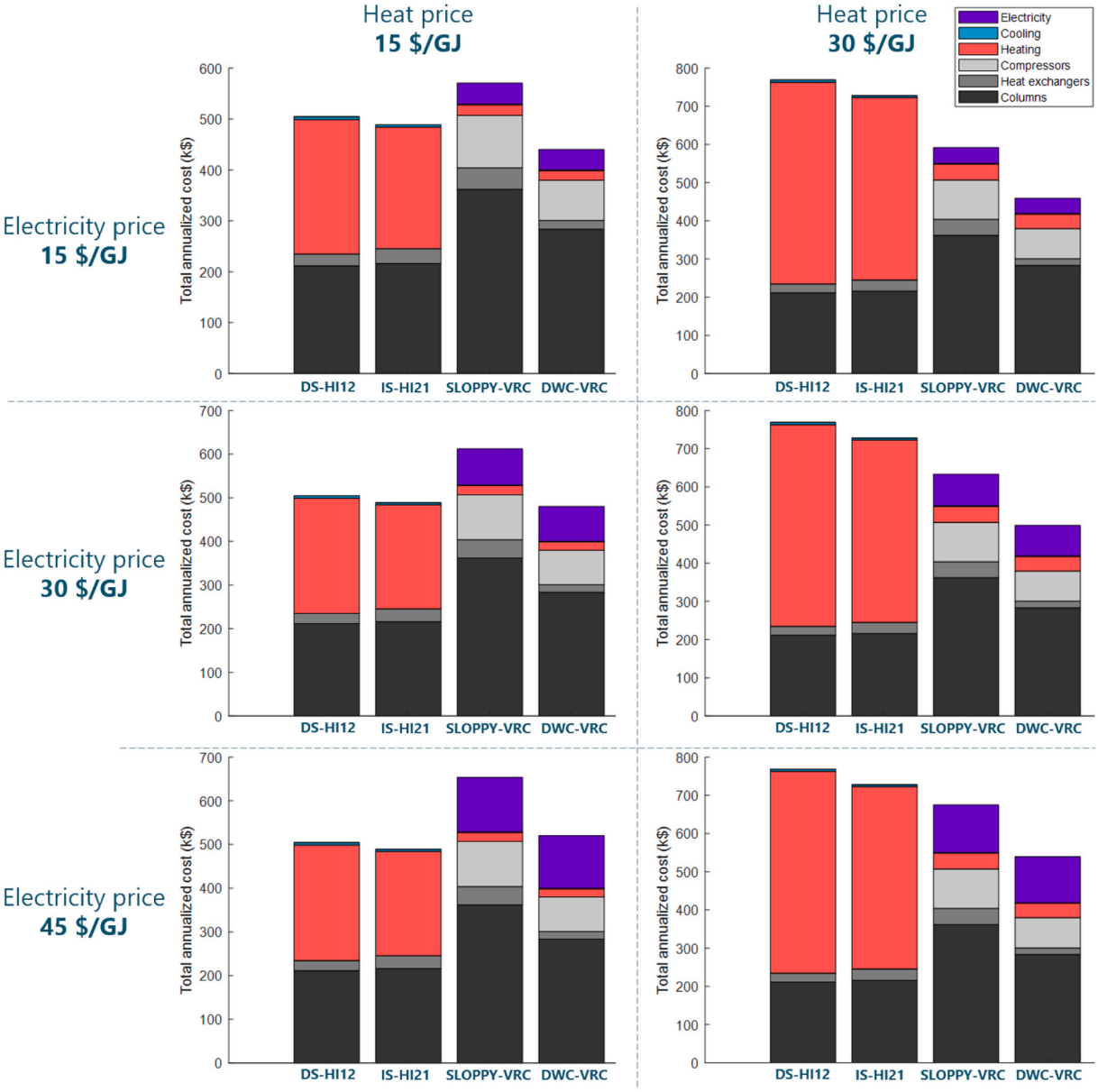

Fig. 16. Sensitivity analysis for total annualized costs of DS-HI12, IS-HI21, SLOPPY-VRC and DWC-VRC with costs for process heat and electricity.

considerable differences in capital and operating cost distribution. While the DS-HI12 and IS-HI21 have the 1st and 2nd lowest capital cost of all processes, contributing about half of their TAC, and the other half of the costs stems from heating. The VRC-assisted processes (SLOPPY-VRC, DWC-VRC) require little energy and operating cost, but require significantly higher investment such that capital costs represent 84–91 % of their TAC.

To systematically study how each configuration responds to changes in utility prices, six scenarios are defined by using process heat prices of 15 $/GJ (0.054 $/kWh) and 30 $/GJ (0.108 $/kWh) at a temperature level of 184 °C and electricity prices of 15 $/GJ, 30 $/GJ and 45 $/GJ (0.162 $/kWh). The TAC and the individual shares are illustrated for the four selected processes in Fig. 16. Note that the capital cost of all processes remains unaffected as the current results represent the economic performance of the process configurations at MED, not an economically optimized design.

At heat prices of 30 $/GJ, the VRC-based options offer the lowest overall TAC for all considered heat prices because their high capital costs are offset by much lower operating costs. The DWC-VRC offers TAC savings of up to 37 % over the IS-HI21 for an electricity price of 15 $/GJ. For heat prices of 15 $/GJ however, the TAC of the HI processes is almost identical to the capital cost of the SLOPPY-VRC due to the high costs for columns and compressors. The DWC-VRC results in marginal TAC savings for electricity prices of 30 $/GJ but allows for TAC savings of 10 % over the IS-HI21 when electricity and heat are priced equally at 15 $/GJ.

While, the electricity-to-heat price ratio is identical for the scenarios where both electricity costs either 15 $/GJ or 30 $/GJ, the ranking changes significantly. Thus, not only the ratio but also the absolute costs of energy are important. The TAC of DWC-VRC only increases by a factor of 1.23 from the lowest to the highest energy costs scenario, whereas the TAC of the IS-HI21 increases by a factor of 1.49, indicating that VRC configurations have more stable TAC for changing energy prices. Thus, they promise beneficial to mitigate the operating cost increase when expecting rising energy prices in the future. Generally, the results are much more sensitive to changing heat prices than changing electricity prices, since even the VRC-assisted configurations require small amounts of heat and little electricity, whereas the HI variants require significates amounts of heat. Ultimately, the choice between a VRC-assisted or a heat-integrated sequence will depend on current and expected energy prices and operational flexibility requirements.

3.2.3. *The influence of depreciation time*

Another important aspect that affects the economic evaluation are the expected depreciation time and interest, which culminate in the capital charge factor (CCF) that is employed to calculate the annualized capital cost. The preceding analysis was based on a depreciation time of 10 years, representing the effective depreciation time for distillation column according to German tax authorities (AfA table), and an interest rate of 6 %, which together yield a CCF of 0.136 (see eq. (9)). To further evaluate the influence of annualized capital costs, different CCF are evaluated, which can be interpreted as different depreciation times of 2 (CCF = 0.545), 8 (CCF = 0.161) and 25 (CCF = 0.078) years at a fixed interest rate of 6 %. The utility prices from Table 1 are again used for this study.

Fig. 17 presents the TAC distribution for the configurations with the ten lowest TAC values for each scenario. Owing to the high capital cost of the compressor, VRC-assisted configurations are heavily penalized by a high capital charge factor, such that each of the best ten configuration ranking for the 2 year depreciation makes use of HI. In four of those configurations direct HI is however supplemented by VRC. The DWC takes only the 13th place ranking regarding TAC, since the cost for the combined column is higher than the entire capital cost of any of the ten lowest-TAC configurations. While the DWC height is again estimated to be almost identical to the combined height of the individual columns of the DS-HI12, the diameter of the DWC is almost twice the diameter of the individual columns, resulting in much larger column costs. Thus, according to the shortcut results, the DWC does not provide considerable capital cost savings over heat integrated sequences benefitting from smaller columns at altered operating pressures. Compared to the non-integrated direct sequence, the DWC however does save 24 % capital cost, which again meets the expectations.

As the depreciation time increases to eight years (cf. Fig. 17 (center), the trade-off between operating and capital cost becomes more balanced. More VRC-assisted configurations are among the top ten TAC options, including the DWC-VRC, as their lower energy demand begins to offset the higher investment cost. Notably, the best two positions are still occupied by the IS-HI21 and DS-HI12 configurations using just direct HI. For an extensive 25-year depreciation period at 6 % interest rate, or alternatively a depreciation period of 15 years with 2 % interest rate, the capital-intensive VRC-assisted processes become dominant, also utilizing multiple VRC connections. The IS-HI21 and DS-HI12 processes remain within the top ten.

Building on the previous discussion, Fig. 18 provides a multi-criteria analysis of the process configurations w.r.t. investment costs and annual operating costs. Each dot in the figure represents a distinct configuration, while the black dots mark the pareto front, resulting from those configurations that are not dominated by any other configuration in both performance metrics, along with illustrative *iso*-TAC lines for specific CCF values. A key observation is that, given constant utility cost, configurations apart from the pareto front can never be optimal in terms of TAC for *any* chosen CCF value.

The *iso*-TAC line indicates how the best configuration in terms of TAC changes with an increasing CCF, as capital-intensive processes become more attractive, since the burden of annualized investment costs is reduced. Conversely, for short depreciation times or higher interest rates, processes with lower investment, even if they have somewhat higher operating costs, yield the lowest TAC.

Looking specifically at the points with similar CCF values as analyzed in Fig. 17, it becomes apparent that for higher CCF, DS-HI12 shows the lowest TAC, while for CCF between 0.244 and 0.103, IS-H21 shows the lowest TAC. For longer depreciation times and lower CCF, the DWC-VRC provides the lowest TAC. Although the sloppy split with three VRC connections has a slightly lower energy operating cost than the DWC-VRC configuration and lies on the pareto front, it would only emerge as the overall TAC optimum for very long depreciation times at unrealistically low interest rates below 1.4 % due to the significantly higher investment costs. The presented screening tool thus allows to rapidly evaluate a large number of process alternatives and pinpoint precisely under which conditions certain configurations become competitive. This capability is invaluable for guiding decisions in dynamic market conditions, where both utility prices and financing terms may vary over time.

4. Conclusion

The current article presents an algorithmic framework for the evaluation of more than 750 simple and energy integrated distillation configurations for separating multicomponent mixtures into three product streams. It covers a wide range of energy integration strategies, including direct heat integration, thermal coupling, dual- and triple-effect distillation, as well as all conceivable VRC-assisted options. It therefore includes hybrid combinations of integration methods, providing a comprehensive evaluation of each process configuration based on minimum energy demand computations. Providing all relevant mass and energy streams, operating pressures and temperatures, equipment sizing and cost estimation can be performed for a multi-criteria analysis, considering the trade-off between investment and operating costs. Opposed to most other shortcut methods, the approach is well-suited for nonideal and azeotropic mixtures as it avoids limiting assumptions of constant relative volatility and constant molar overflow.

The framework's computational efficiency and versatility are

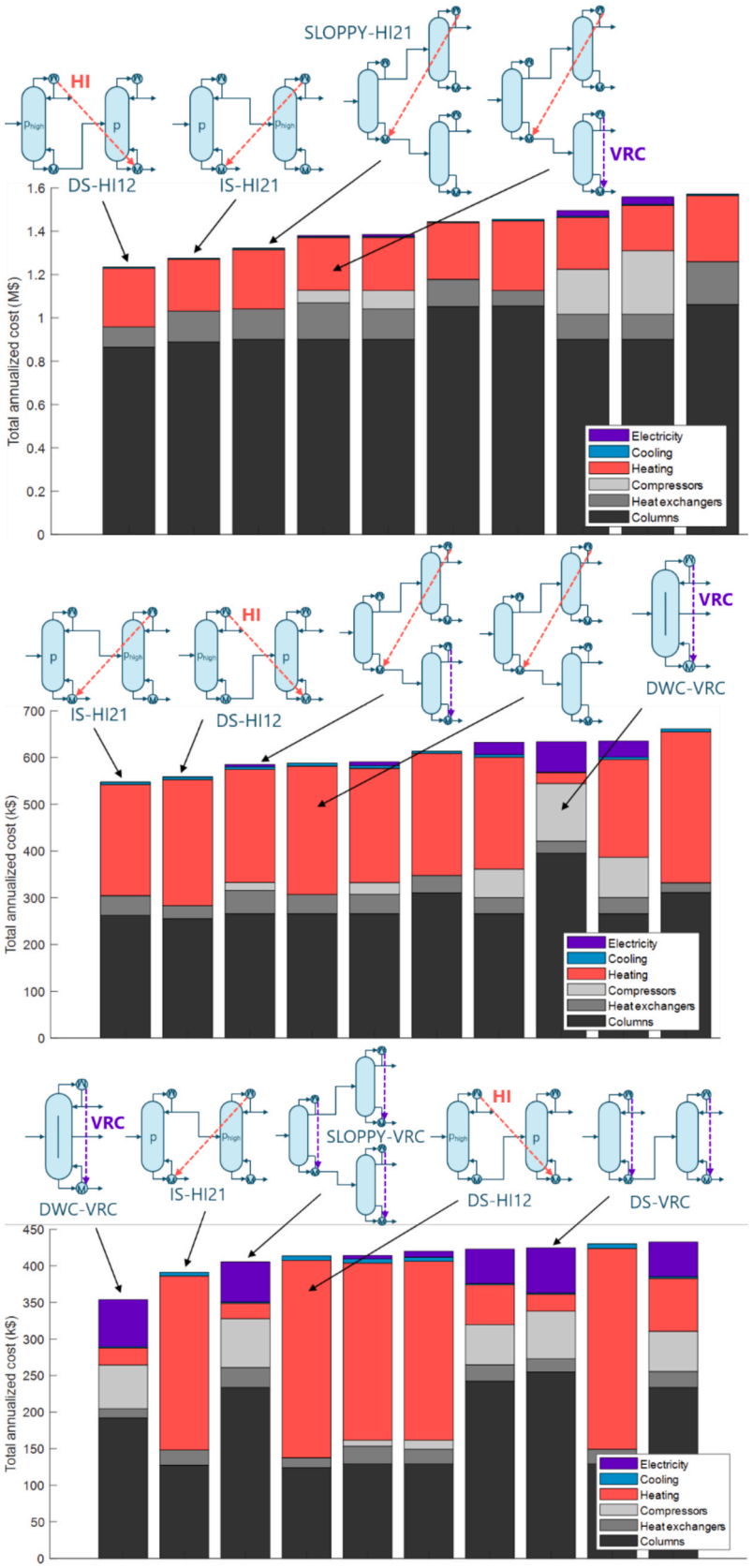

Fig. 17. Distribution of TAC for 10 practically feasible sequences with lowest TAC for a depreciation time of 2 years (top), 8 years (center) and 25 years (bottom).

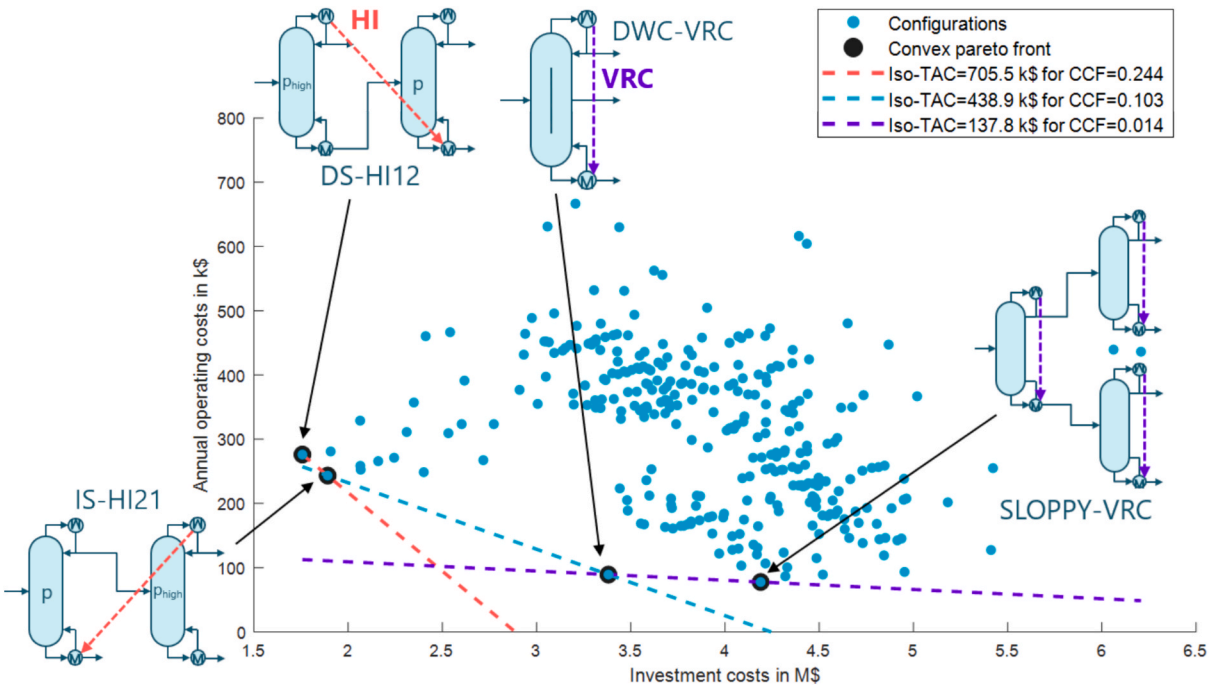

Fig. 18. Trade-off between operating costs and investment costs for practically feasible sequences with highlighted pareto-optimal solutions and *iso*-TAC lines with given CCF.

demonstrated through its ability to screen hundreds of process variants in few minutes of computational time on a conventional desktop computer. This computational efficiency enables complex sensitivity analyses for uncertain process conditions, thermodynamic models, and varied economic or utility scenarios, which allows design engineers to rapidly identify the most promising process alternatives under different operating and market conditions and the most sensitive data that requires accurate parameters. Notably, the analysis reveals that oftentimes favored designs, such as dividing wall columns, are not generally the best choice when evaluated within a broader and more integrated design space. Once the most promising candidates are identified, rigorous MESH-based process optimization can be applied in subsequent design steps to provide more detailed process designs [88].

The framework will further be extended to include additional configurations, such as the aforementioned liquid-only transfer variants for thermal coupling without vapor transfer [18], which can further be combined with heat integration. Individual evaluations of side-rectifier and side-stripper configurations have already demonstrated the potential for significant energy and cost savings [18,58]. Furthermore, extensions towards an improved flash-enhanced VRC scheme that utilizes a vapor recycle to enable full electrification and closed-cycle heat-pumps [24] will be considered. Ongoing work is also focused on incorporating exergetic efficiency calculations and exergy loss metrics into the multi-criteria analysis, also in order to also account for the quality of the energy used. Finally, the framework may also be extended to separations that consider more than three products.

Declaration of generative AI and AI-assisted technologies in the writing process

During the preparation of this work the authors used ChatGPT in order to aid in formulation of text sections. After using this tool/service, the authors reviewed and edited the content as needed and take full responsibility for the content of the publication.

CRediT authorship contribution statement

Momme Adami: Writing – review & editing, Writing – original draft, Validation, Software, Project administration, Methodology, Investigation, Data curation, Conceptualization. **Dennis Espert:** Validation, Software, Methodology. **Mirko Skiborowski:** Writing – review & editing, Supervision, Software, Resources, Methodology.

Declaration of competing interest

The authors declare that they have no known competing financial interests or personal relationships that could have appeared to influence the work reported in this paper.

Acknowledgements

This research did not receive any specific grant from funding agencies in the public, commercial, or not-for-profit sectors.

Appendix A. Supplementary data

Supplementary data to this article can be found online at https://doi.org/10.1016/j.seppur.2025.134463.

Data availability

Data will be made available on request.

References

[1] A. Marina, S. Spoelstra, H.A. Zondag, A.K. Wemmers, An estimation of the European industrial heat pump market potential, Renew. Sustain. Energy Rev. 139 (2021) 110545, https://doi.org/10.1016/j.rser.2020.110545.
[2] D.S. Sholl, R.P. Lively, Seven chemical separations to change the world, Nature 532 (7600) (2016) 435–437, https://doi.org/10.1038/532435a.
[3] R.C. van Diggelen, A.A. Kiss, A.W. Heemink, Comparison of control strategies for dividing-wall columns, Ind. Eng. Chem. Res. 49 (1) (2010) 288–307, https://doi.org/10.1021/ie9010673.
[4] P.C. Wankat, Separation process engineering, 2nd ed., Prentice Hall, Upper Saddle River, NJ, 2007.

[5] R.T. Gooty, J.A.C. Velasco, R. Agrawal, Methods to assess numerous distillation schemes for binary mixtures, Chem. Eng. Res. Des. 172 (2021) 1–20, https://doi.org/10.1016/j.cherd.2021.05.022.

[6] E.L. Cussler, B.K. Dutta, On separation efficiency, AIChE J. 58 (12) (2012) 3825–3831, https://doi.org/10.1002/aic.13779.

[7] M. Blahušiak, A.A. Kiss, K. Babic, S.R. Kersten, G. Bargeman, B. Schuur, Insights into the selection and design of fluid separation processes, Sep. Purif. Technol. 194 (2018) 301–318, https://doi.org/10.1016/j.seppur.2017.10.026.

[8] M. Skiborowski, K. F. Kruber, T. Waltermann, Sustainable distillation processes, in: Sustainable Separation Engineering, G. Szekely and D. Zhao, Eds.: Wiley, 2022, pp. 431–481.

[9] A. Rix, C. Hecht, N. Paul, J. Schallenberg, Design of heat-integrated columns: industrial practice, Chem. Eng. Res. Des. 147 (2019) 83–89, https://doi.org/10.1016/j.cherd.2019.05.009.

[10] C. Cui, Z. Xi, S. Liu, J. Sun, An enumeration-based synthesis framework for multi-effect distillation processes, Chem. Eng. Res. Des. 144 (2019) 216–227, https://doi.org/10.1016/j.cherd.2019.02.018.

[11] Z. Shen, Q. Qu, M. Chen, H. Lyu, J. Sun, Advancements in methanol distillation system: a comprehensive overview, Chem. Eng. Res. Des. 199 (2023) 130–151, https://doi.org/10.1016/j.cherd.2023.09.026.

[12] A. Al-Karaghouli, L.L. Kazmerski, Energy consumption and water production cost of conventional and renewable-energy-powered desalination processes, Renew. Sustain. Energy Rev. 24 (2013) 343–356, https://doi.org/10.1016/j.rser.2012.12.064.

[13] R. Agrawal, Z.T. Fidkowski, Are thermally coupled distillation columns always thermodynamically more efficient for ternary distillations? Am. Chem. Soc. 37 (1998) 3444–3454.

[14] G. Kaibel, Energieintegration in der thermischen Verfahrenstechnik, Chem. Ing. Tech. 62 (2) (1990) 99–106, https://doi.org/10.1002/cite.330620206.

[15] G. Lukač, I.J. Halvorsen, Ž. Olujić, I. Dejanović, On controllability of a fully thermally coupled four-product dividing wall column, Chem. Eng. Res. Des. 147 (2019) 367–377, https://doi.org/10.1016/j.cherd.2019.04.041.

[16] A.A. Kiss, Distillation technology - still young and full of breakthrough opportunities, J. Chem. Technol. Biotechnol. 89 (4) (2014) 479–498, https://doi.org/10.1002/jctb.4262.

[17] T. Waltermann, S. Sibbing, M. Skiborowski, Optimization-based design of dividing wall columns with extended and multiple dividing walls for three- and four-product separations, Chem. Eng. Process. - Process Intesif. 146 (2019) 107688, https://doi.org/10.1016/j.cep.2019.107688.

[18] A.S. Horsch, M. Skiborowski, Thermally coupled distillation columns without vapor transfer – current state and further needs, Sep. Purif. Technol. 354 (2025) 128762, https://doi.org/10.1016/j.seppur.2024.128762.

[19] R. Agrawal, Thermally coupled distillation with reduced number of intercolumn vapor transfers, AIChE J. 46 (11) (2000) 2198–2210, https://doi.org/10.1002/aic.690461112.

[20] G.M. Ramapriya, M. Tawarmalani, R. Agrawal, Thermal coupling links to liquid-only transfer streams: an enumeration method for new FTC dividing wall columns, AIChE J. 62 (4) (2016) 1200–1211, https://doi.org/10.1002/aic.15053.

[21] R. Agrawal, Multieffect distillation for thermally coupled configurations, AIChE J. 46 (11) (2000) 2211–2224, https://doi.org/10.1002/aic.690461113.

[22] A.K. Jana, Heat integrated distillation operation, Appl. Energy 87 (5) (2010) 1477–1494, https://doi.org/10.1016/j.apenergy.2009.10.014.

[23] A. Rix, M. Schröder, N. Paul, Vapor recompression: an interesting option for vacuum columns? Chem. Eng. Res. Des. 191 (2023) 226–235, https://doi.org/10.1016/j.cherd.2023.01.030.

[24] M. Adami, J. Schnurr, M. Skiborowski, Electrified distillation – optimized design of closed cycle heat pumps with refrigerant selection and flash-enhanced mechanical vapor recompression, Appl. Therm. Eng. (2025) 126559, https://doi.org/10.1016/j.applthermaleng.2025.126559.

[25] C.S. Gan, W.-T. Tang, J.D. Ward, Combinatorial energy intensification of a ternary distillation process, Chem. Eng. Process. - Process Intesif. 204 (2024) 109952, https://doi.org/10.1016/j.cep.2024.109952.

[26] L. Xu, M. Li, X. Yin, X. Yuan, New intensified heat integration of vapor recompression assisted dividing wall column, Ind. Eng. Chem. Res. 56 (8) (2017) 2188–2196, https://doi.org/10.1021/acs.iecr.6b03802.

[27] C. Cui, H. Yin, J. Yang, D. Wei, J. Sun, C. Guo, Selecting suitable energy-saving distillation schemes: making quick decisions, Chem. Eng. Process. - Process Intesif. 107 (2016) 138–150, https://doi.org/10.1016/j.cep.2016.05.009.

[28] A.A. Kiss, S.J. Flores Landaeta, C.A. Infante Ferreira, Towards energy efficient distillation technologies – making the right choice, Energy 47 (1) (2012) 531–542, https://doi.org/10.1016/j.energy.2012.09.038.

[29] R.W. Thompson, C.J. King, Systematic synthesis of separation schemes, AIChE J. 18 (5) (1972) 941–948, https://doi.org/10.1002/aic.690180510.

[30] T.J. Mathew, et al., Optimization of distillation configurations for multicomponent-product distillations, Comput. Chem. Eng. 184 (2024) 108628, https://doi.org/10.1016/j.compchemeng.2024.108628.

[31] Z. Jiang, M. Tawarmalani, R. Agrawal, Minimum reflux calculation for multicomponent distillation in multi-feed, multi-product columns: Mathematical model, AIChE J. 68 (12) (2022), https://doi.org/10.1002/aic.17929.

[32] R. Agrawal, Synthesis of multicomponent distillation column configurations, AIChE J. 49 (2) (2003) 379–401.

[33] Z. Jiang, G. Madenoor Ramapriya, M. Tawarmalani, R. Agrawal, Minimum energy of multicomponent distillation systems using minimum additional heat and mass integration sections, AIChE J. 64 (9) (2018) 3410–3418, https://doi.org/10.1002/aic.16189.

[34] V.H. Shah, R. Agrawal, A matrix method for multicomponent distillation sequences, AIChE J. 56 (7) (2010) 1759–1775, https://doi.org/10.1002/aic.12118.

[35] U. Nallasivam, V.H. Shah, A.A. Shenvi, J. Huff, M. Tawarmalani, R. Agrawal, Global optimization of multicomponent distillation configurations: 2 Enumeration Based Global Minimization Algorithm, AIChE J. 62 (6) (2016) 2071–2086, https://doi.org/10.1002/aic.15204.

[36] Z. Jiang, Z. Chen, J. Huff, A.A. Shenvi, M. Tawarmalani, R. Agrawal, Global minimization of total exergy loss of multicomponent distillation configurations, AIChE J. 65 (11) (2019), https://doi.org/10.1002/aic.16737.

[37] Z. Jiang, et al., Global optimization of multicomponent distillation configurations: Global minimization of total cost for multicomponent mixture separations, Comput. Chem. Eng. 126 (2019) 249–262, https://doi.org/10.1016/j.compchemeng.2019.04.009.

[38] M.R. Fenske, Fractionation of straight-run Pennsylvania gasoline, Ind. Eng. Chem. 24 (5) (1932) 482–485, https://doi.org/10.1021/ie50269a003.

[39] A.S. Nogaja, T.J. Mathew, M. Tawarmalani, R. Agrawal, Identifying heat-integrated energy-efficient multicomponent distillation configurations, Ind. Eng. Chem. Res. 61 (37) (2022) 13984–13995, https://doi.org/10.1021/acs.iecr.2c00870.

[40] A. Wei-zhong, Y. Xi-Gang, A simulated annealing-based approach to the optimal synthesis of heat-integrated distillation sequences, Comput. Chem. Eng. 33 (1) (2009) 199–212, https://doi.org/10.1016/j.compchemeng.2008.08.001.

[41] S. Zhang, Y. Luo, X. Yuan, Synthesis of simultaneously heat integrated and thermally coupled nonsharp distillation sequences based on stochastic optimization, Comput. Chem. Eng. 127 (2019) 158–174, https://doi.org/10.1016/j.compchemeng.2019.05.028.

[42] Q. Li, A.J. Finn, S.J. Doyle, R. Smith, A.A. Kiss, Synthesis and optimization of energy integrated advanced distillation sequences, Sep. Purif. Technol. 315 (2023) 123717, https://doi.org/10.1016/j.seppur.2023.123717.

[43] A.J.V. Underwood, Fractional distillation of ternary mixtures, Part I, J. Inst. Petroleum (1945) 111–118.

[44] A.J.V. Underwood, Fractional distillation of ternary mixtures, Part II, J. Inst. Petroleum (1945) 598–613.

[45] A.J.V. Underwood, Fractional distillation of multicomponent mixtures-calculation of minimum reflux ratio, J. Inst. Petroleum 1 (1946) 614–626.

[46] G.M. Ramapriya, A. Selvarajah, L.E. Jimenez Cucaita, J. Huff, M. Tawarmalani, R. Agrawal, Short-cut methods versus rigorous methods for performance-evaluation of distillation configurations, Ind. Eng. Chem. Res. 57 (22) (2018) 7726–7731, https://doi.org/10.1021/acs.iecr.7b05214.

[47] T.J. Mathew, M. Tawarmalani, R. Agrawal, Relaxing the constant molar overflow assumption in distillation optimization, AIChE J. (2023), https://doi.org/10.1002/aic.18125.

[48] W.-T. Tang, J.D. Ward, Comparison of separation alternatives for two industrial C6–C7 aliphatic hydrocarbon mixtures including stacked complex sequences, Ind. Eng. Chem. Res. 61 (36) (2022) 13488–13504, https://doi.org/10.1021/acs.iecr.2c00756.

[49] Z. Mekidiche, J.A. Labarta, J. Javaloyes-Anton, J.A. Caballero, From power to heat: strategies for electrifying distillation for sustainable chemical processes, Appl. Therm. Eng. 257 (2024) 124316, https://doi.org/10.1016/j.applthermaleng.2024.124316.

[50] K. Kruber, S. Kinau, M. Skiborowski, Chapter 9 Hybrid optimization methodologies for the design of chemical processes, in: F. I. Gómez-Castro, V. Rico-Ramírez (Eds.) Optimization in Chemical Engineering, : De Gruyter, 2025, pp. 305–342.

[51] M.-O. Bertran, R. Frauzem, A.-S. Sanchez-Arcilla, L. Zhang, J.M. Woodley, R. Gani, A generic methodology for processing route synthesis and design based on superstructure optimization, Comput. Chem. Eng. 106 (2017) 892–910, https://doi.org/10.1016/j.compchemeng.2017.01.030.

[52] M. Skiborowski, A. Harwardt, W. Marquardt, Conceptual design of distillation-based hybrid separation processes, Annu. Rev. Chem. Biomol. Eng. 4 (2013) 45–68, https://doi.org/10.1146/annurev-chembioeng-061010-114129.

[53] M. Skiborowski, J. Wessel, W. Marquardt, Efficient optimization-based design of membrane-assisted distillation processes, Ind. Eng. Chem. Res. 53 (40) (2014) 15698–15717, https://doi.org/10.1021/ie502482b.

[54] K. Kraemer, S. Kossack, W. Marquardt, Efficient optimization-based design of distillation processes for homogeneous azeotropic mixtures, Ind. Eng. Chem. Res. 48 (14) (2009) 6749–6764, https://doi.org/10.1021/ie900143e.

[55] M. Skiborowski, A. Harwardt, W. Marquardt, Conceptual design of azeotropic distillation processes, in Distillation: Elsevier, 2014, pp. 305–355.

[56] S. Brüggemann, W. Marquardt, Rapid screening of design alternatives for nonideal multiproduct distillation processes, Comput. Chem. Eng. 29 (1) (2004) 165–179, https://doi.org/10.1016/j.compchemeng.2004.07.009.

[57] M. Skiborowski, Fast screening of energy and cost efficient intensified distillation processes, Chem. Eng. Trans. 69 (2018) 199–204, https://doi.org/10.3303/CET1869034.

[58] M. Skiborowski, Energy efficient distillation by combination of thermal coupling and heat, Integration 48 (2020) 991–996, https://doi.org/10.1016/B978-0-12-823377-1.50166-X.

[59] M. Adami, A.S. Horsch, M. Skiborowski, Can simple side stream configurations compete with fully thermally coupled dividing wall columns?, in: The 12th international conference Distillation & Absorption, 2022.

[60] R. Agrawal, Z.T. Fidkowski, Ternary distillation schemes with partial reboiler or partial condenser, Ind. Eng. Chem. Res. 37 (8) (1998) 3455–3462, https://doi.org/10.1021/ie980063e.

[61] F.W. Winn, New relative volatility method for distillation calculations, Petrol. Refin 37 (5) (1958) 216–218.

[62] K.M. Guthrie, Data and techniques for preliminary capital cost estimating, Chem. Eng. 76 (1969) 114–142.
[63] L.T. Biegler, I.E. Grossmann, A.W. Westerberg, Systematic Methods of Chemical Process Design, Prentice Hall PTR, Upper Saddle River, New Jersey, 1997.
[64] J. Bausa, R. von Watzdorf, W. Marquardt, Shortcut methods for nonideal multicomponent distillation: I. Simple columns, AIChE J. 44 (10) (1998) 2181–2198, https://doi.org/10.1002/aic.690441008.
[65] AVT.SVT at RWTH Aachen University, Process Synthesis Softwarecollection: Process Analysis and Design Routines. Aachen, 2014. Accessed: Feb. 10 2025. [Online]. Available: https://www.avt.rwth-aachen.de/cms/avt/forschung/sonstiges/software/~iptu/softwaresammlung-prozesssynthese/?lidx=1.
[66] R. von Watzdorf, J. Bausa, W. Marquard, Shortcut methods for nonideal multicomponent distillation: 2. Complex Columns, AIChE J. 45 (8) (1999) 1615–1628.
[67] N.A. Carlberg, A.W. Westerberg, Temperature-heat diagrams for complex columns. 2. Underwood's method for side strippers and enrichers, Ind. Eng. Chem. Res. 28 (9) (1989) 1379–1386, https://doi.org/10.1021/ie00093a017.
[68] M.A. Navarro, J. Javaloyes, J.A. Caballero, I.E. Grossmann, Strategies for the robust simulation of thermally coupled distillation sequences, Comput. Chem. Eng. 36 (2012) 149–159, https://doi.org/10.1016/j.compchemeng.2011.06.014.
[69] Y. Li, Y. Gao, G. Li, Y. Zheng, H. Pan, H. Ling, An effective procedure for optimized design of heat pump distillation process, Chem. Eng. Process. - Process Intesif. 208 (2025) 110096, https://doi.org/10.1016/j.cep.2024.110096.
[70] G. Modla, P. Lang, Decrease of the energy demand of distillation with vapour recompression, in: Proceedings of the 5th international scientific conference on advances in mechanical engineering (ISCAME 2017) Debrecen, Hungary, 2017.
[71] C. Cui, X. Zhang, M. Qi, H. Lyu, J. Sun, A.A. Kiss, Fully electrified heat pump assisted distillation process by flash vapour circulation, Chem. Eng. Res. Des. 206 (2024) 280–284, https://doi.org/10.1016/j.cherd.2024.05.011.
[72] A.S. Nogaja, M. Tawarmalani, R. Agrawal, Cogeneration improves separation efficiency, Ind. Eng. Chem. Res. 63 (43) (2024) 18564–18574, https://doi.org/10.1021/acs.iecr.4c03190.
[73] J. Bausa, R. Watzdorf, W. Marquardt, Minimum energy demand for nonideal multicomponent distillations in complex columns, Comput. Chem. Eng. 20 (1996) S55–S60, https://doi.org/10.1016/0098-1354(96)00020-8.
[74] S. Brüggemann, Rapid Screening of Conceptual Design Alternatives for Distillation Processes, Düsseldorf, 2005.
[75] I.J. Halvorsen, S. Skogestad, Minimum Energy Consumption in Multicomponent Distillation. 2. Three-Product Petlyuk Arrangements, Ind. Eng. Chem. Res. 42 (3) (2003) 605–615, https://doi.org/10.1021/ie0108649.
[76] R. Turton, R. C. Bailie, W. B. Whiting, J. A. Shaeiwitz, Analysis, synthesis, and design of chemical processes, 3rd ed. Upper Saddle River, New Jersey: Pearson Education [distributor], 2009.
[77] L.T. Biegler, Systematic methods of chemical process design, Prentice Hall PTR, Upper Saddle River, N.J., 1997.
[78] G. Towler, R. Sinnot, Chemical engineering design. Principles, practice and economics of plant and process design. Amsterdam, Boston, Heidelberg, London, New York, Oxford, Paris, San Diego, San Francisco, Singapore, Sydney, Tokio: Elsevier/Butterworth-Heinemann, 2008.
[79] J.M. Douglas, Conceptual design of chemical processes, McGraw-Hill Publishing Company, New York, 1988.
[80] Y.H. Kim, Energy savings in the benzene-toluene-xylene separation process using an extended divided-wall column, Chem. Eng. Technol. 39 (12) (2016) 2312–2322, https://doi.org/10.1002/ceat.201500605.
[81] M.M. Donahue, B.J. Roach, J.J. Downs, T. Blevins, M. Baldea, R.B. Eldridge, Dividing wall column control: common practices and key findings, Chem. Eng. Process. - Process Intesif. 107 (2016) 106–115, https://doi.org/10.1016/j.cep.2016.05.013.
[82] L.-M. Ränger, I.J. Halvorsen, T. Grützner, S. Skogestad, What can go wrong in a dividing wall column and how to detect it, Sep. Purif. Technol. 354 (2025) 129151, https://doi.org/10.1016/j.seppur.2024.129151.
[83] C. Cui, Q. Zhang, X. Zhang, J. Sun, Eliminating the vapor split in dividing wall columns through controllable double liquid-only side-stream distillation configuration, Sep. Purif. Technol. 242 (2020) 1–15, https://doi.org/10.1016/j.seppur.2020.116837.
[84] C. Cui, X. Zhang, J. Sun, Design and optimization of energy-efficient liquid-only side-stream distillation configurations using a stochastic algorithm, Chem. Eng. Res. Des. 145 (2019) 48–52, https://doi.org/10.1016/j.cherd.2019.03.001.
[85] T. Waltermann, M. Skiborowski, Conceptual design of highly integrated processes - optimization of dividing wall columns, Chem. Ing. Tech. 89 (5) (2017) 562–581, https://doi.org/10.1002/cite.201600128.
[86] Statista, Industriestrompreise (inklusive Stromsteuer) in Deutschland in den Jahren 1998 bis 2024. [Online]. Available: https://de.statista.com/statistik/daten/studie/252029/umfrage/industriestrompreise-inkl-stromsteuer-in-deutschland/ (accessed: Mar. 18 2025).
[87] Statista, Gaspreise für Gewerbe- und Industriekunden in Deutschland in den Jahren 2008 bis 2024. [Online]. Available: https://de.statista.com/statistik/daten/studie/168528/umfrage/gaspreise-fuer-gewerbe-und-industriekunden-seit-2006/ (accessed: Mar. 18 2025).
[88] M. Skiborowski, A. Harwardt, W. Marquardt, Efficient optimization-based design for the separation of heterogeneous azeotropic mixtures, Comput. Chem. Eng. 72 (5) (2015) 34–51, https://doi.org/10.1016/j.compchemeng.2014.03.012.